

**HETEROGENEOUS REACTION OF NO₂ ON SOOT SURFACES
AND THE EFFECT OF SOOT AGING ON ITS REACTIVITY
LEADING TO HONO FORMATION**

A Thesis

by

MIGUEL CRUZ QUIÑONES

Submitted to the Office of Graduate Studies of
Texas A&M University
in partial fulfillment of the requirements for the degree of

MASTER OF SCIENCE

December 2009

Major Subject: Chemistry

**HETEROGENEOUS REACTION OF NO₂ ON SOOT SURFACES
AND THE EFFECT OF SOOT AGING ON ITS REACTIVITY
LEADING TO HONO FORMATION**

A Thesis

by

MIGUEL CRUZ QUIÑONES

Submitted to the Office of Graduates Studies of
Texas A&M University
in partial fulfillment of the requirements for the degree of
MASTER OF SCIENCE

Approved by:

Chair of Committee,	Renyi Zhang
Committee Members,	Sarah D. Brooks
	Robert R. Lucchese
	Simon W. North
Head of Departments,	David H. Russell

December 2009

Major Subject: Chemistry

ABSTRACT

Heterogeneous Reaction of NO₂ on Soot Surfaces and the Effect of Soot Aging on Its Reactivity Leading to HONO Formation. (December 2009)

Miguel Cruz Quiñones, B.S., University of Puerto Rico at Río Piedras

Chair of Advisory Committee: Dr. Renyi Zhang

Soot aerosols are known to be an important atmospheric constituent. The physical and chemical properties of soot allows it to act as a precursor of gas-surface heterogeneous reactions, providing active sites for the reduction and oxidation of trace species in the atmosphere, potentially affecting atmospheric composition. In this work the heterogeneous reaction of NO₂ on soot leading to nitrous acid (HONO) formation was studied through a series of kinetic uptake experiments and HONO yield measurements. The soot was collected from a diffusion flame using propane and kerosene fuels using two different methods. A low pressure fast-flow reactor coupled to a Chemical Ionization Mass Spectrometer (CIMS) was used to monitor NO₂ and HONO signals evolution using atmospheric-level NO₂ concentration. HONO yields up to 100% were measured and NO₂ uptake coefficients varying from 5.6×10^{-6} to 1.6×10^{-4} were obtained. Heating soot samples before exposure to NO₂ increased HONO yield and the NO₂ uptake coefficient on soot due to the removal of the organic fraction from the soot backbone unblocking active sites, which become accessible for the heterogeneous reaction. From the kinetic uptake curves and the effect observed in the HONO yield and

NO_2 uptake coefficient measurements by heating the soot samples, our results support a complex oxidation-reduction mechanism of reaction. This heterogeneous reaction mechanism involves a combination of competitive adsorptive and reductive centers on soot surface where NO_2 is converted into HONO, and the presence of processes on soot where HONO can be decomposed producing other products. Atmospheric soot “aging” effect on the reactivity of soot toward NO_2 and HONO yield was studied by coating the soot surface with glutaric acid, succinic acid, sulfuric acid, and pyrene. Glutaric and succinic acid increased both HONO yield and the NO_2 uptake coefficients, while sulfuric acid decreased both. However, pyrene did not show any particular trend.

ACKNOWLEDGEMENTS

I would like to take this opportunity to acknowledge my committee chair, Dr. Renyi Zhang, for all his advise and support throughout this journey. I would like to thank Texas Environmental Research Consortium (TERC) and Houston Advanced Research Center (HARC) for providing funding for this research. Special thanks go to Alexei Khalizov for all his valuable effort, useful discussions, and assistance in any problem that I encountered along the way and Dr. Sarah D. Brooks for allowing me to use her lab facilities. Ling Wang and the rest of Dr. Zhang's research group is also acknowledged. Thank you guys for your support and suggestions.

I cannot finish without thanking my family and fiancé for their unconditional love, support, and encouragement, which gave me the strength to complete this goal. I am grateful to God for giving me so many blessings and for the opportunity of meeting such wonderful people through this memorable experience. Without them, this work would not have been possible.

TABLE OF CONTENTS

	Page
ABSTRACT.....	iii
ACKNOWLEDGEMENTS.....	v
TABLE OF CONTENTS.....	vi
LIST OF TABLES.....	vii
LIST OF FIGURES.....	viii
1. INTRODUCTION.....	1
1.1. Important of Soot in the Atmosphere.....	1
1.2. Role of Nitrous Acid in the Urban Environments and the Reaction of NO ₂ with Soot as Its Main Source.....	4
2. EXPERIMENTAL.....	11
2.1. Preparation of Soot Samples.....	11
2.2. NO ₂ Uptake and HONO Yield Measurements.....	12
2.3. Soot Coating with Different Vapors.....	16
2.4. Soot Characterization by ATR-FTIR Spectroscopy.....	18
3. RESULTS AND DISCUSSION.....	21
3.1. NO ₂ Uptake and HONO Yields on Different Types of Soot.....	21
3.2. Mechanism of NO ₂ Uptake and HONO Production.....	33
3.3. Effect of Coated Soot on the NO ₂ Uptake Coefficients and HONO Yields and Possible Atmospheric Implications.....	36
3.4. Possible Atmospheric Implications.....	42
4. CONCLUSIONS.....	52
REFERENCES AND NOTES.....	56
VITA.....	60

LIST OF TABLES

TABLES	Page
1 Coating Materials.....	10
2 Summary of BET Specific Surface Areas.....	31
3 NO ₂ Uptakes Coefficients (γ) and HONO Yields for Fresh Soot and Coated with Glutaric Acid.....	50
4 NO ₂ Uptakes and HONO Yields for Fresh Soot and Coated with Succinic Acid.....	50
5 NO ₂ Uptakes and HONO Yields for Fresh Soot and Coated with H ₂ SO ₄	51
6 NO ₂ Uptakes and HONO Yields for Fresh Soot and Coated with Pyrene.....	51

LIST OF FIGURES

FIGURE	Page
1	Diagram of the Low-Pressure Fast Flow Reactor-CIMS System Setup..... 13
2	Diagram of the Glass Evacuated Container Where Soot Was Coated..... 20
3	Temporal Profile of NO ₂ Uptake and HONO Production on Type A (a) and Type B (b) Fresh Kerosene Soot with Stepwise Exposure in 2 cm Increments up to 8 cm in Length of 5 and 10 mg of Soot Respectively..... 22
4	Temporal Profile of NO ₂ Uptake and HONO Production on Type A (a) and Type B (b) Fresh Propane Soot with Stepwise Exposure in 2 cm Increments up to 8 cm in Length of 16 and 7 mg of Soot Respectively..... 23
5	Temporal Profile of NO ₂ Uptake and HONO Production on 16 mg of Pre-heated Type A Propane Soot with Stepwise Exposure in 2 cm Increments up to 8 cm in Length..... 28
6	ATR-FTIR Spectra of Type A and Type B Propane Soot Deposited on a ZnSe Crystal Plate, Before and After Heating the Soot Sample to 300 °C in Vacuum for 30 Min..... 29
7	Summary of HONO Yields Determined from the Heterogeneous Reaction of NO ₂ with Fresh Type A Kerosene Soot (Square), Type A Propane Soot (Triangle), Type B Kerosene Soot (Circle), and Type B Propane Soot (Cross) as a Function of Soot Mass..... 29
8	Summary of HONO Yields Determined from the Heterogeneous Reaction of NO ₂ with Pre-heated Type A Kerosene Soot (Square), Type A Propane Soot (Triangle), Type B Kerosene Soot (Circle), and Type B Propane Soot (Cross) as a Function of Soot Mass..... 30
9	Natural Log of NO ₂ ⁻ Signal as a Function of Injector Position on 9 mg of Type B Kerosene Soot Sample, Fresh (a) and Pre-heated to 300 °C for 30 Min in Vacuum (b)..... 31
10	NO ₂ Uptake Coefficients for Fresh (Triangle) and Preheated (Square) Soot as a Function of Soot Mass for the Different Types of Soot Including Type A Kerosene Soot (a), Type A Propane Soot (b), Type B Kerosene Soot (c), and Type B Propane Soot..... 33

FIGURE	Page
11 Temporal Profile of Glutaric Acid with Temporary Exposure to 4 mg of Type A Kerosene Soot over 8 cm in Length.....	37
12 ATR-FTIR Spectra of Type B Kerosene Soot Deposited on a ZnSe Crystal Plate Before and After Exposure to Glutaric Acid Vapor.....	38
13 Temporal Profile of NO ₂ Uptake and HONO Production on 3 mg of Type B Propane Soot, Fresh (a) and Coated with Glutaric Acid at 85 °C in Vacuum for 30 Min (b) with Stepwise Exposure in 2 cm Increments up to 8 cm in Length.....	43
14 Temporal Profile of NO ₂ Uptake and HONO Production on 2 mg of Type B Kerosene Soot, Fresh (a) and Coated with Sulfuric Acid at 85 °C in Vacuum for 30 min (b) with Stepwise Exposure in 2 cm Increments up to 8 cm in Length.....	44
15 Temporal Profile of NO ₂ Uptake and HONO Production on 2 mg of Type B Kerosene Soot, Sulfuric Acid-coated Soot Exposed to 100% RH (a) and Pre-heated (b) with Stepwise Exposure in 2 cm Increments up to 8 cm in Length.....	45
16 Flux of HONO Molecules as a Function of Time During ~1 hr Exposure of 1.68 mg of Type B Propane Soot to the NO ₂ Flow, for a Fresh (a) and Pre-heated Soot (b) with Initial Exposure of 8 cm in Length.....	48
17 Flux of HONO Molecules as a Function of Time During ~1 hr Exposure of 2.88 mg of Glutaric Acid Coated-type B Propane Soot to the NO ₂ Flow (a), and Instant HONO Yield as a Function of Time (b) with Initial Exposure of 8 cm in Length.....	49

1. INTRODUCTION

1.1. Importance of Soot in the Atmosphere

Atmospheric aerosols affect the radiative properties of Earth's atmosphere in various ways: i) through light absorption and scattering of solar radiation¹, and ii) indirectly by promoting cloud formation by acting as cloud condensation nuclei (CCN).² The absorption of radiation, both solar and infrared, by some particles have the effect of warming the atmosphere, while the scattering of solar radiation has a cooling effect by reflecting solar radiation away from the Earth's surface. These phenomena can cause aerosols to impact global climate on a large time scale.^{3,4} Furthermore, it has been shown that high concentration of fine particles in the lower stratosphere results in respiratory health effects and decrease visibility.⁵ A type of carbonaceous aerosol of particular interest due to its potential to affect atmospheric composition is soot, which consists primarily of black carbon with variable fraction of organic materials. Soot aerosol originates from incomplete combustion of fossil fuels and biomass burning. Globally, large amounts of soot aerosol are emitted, with an average emission rate of 8 to 24 Tg of carbon per year (Tg yr^{-1}).^{6,7}

Anthropogenic sources such as industrial process and combustion engines, as well as biomass burning, are the main soot sources in urban areas. Loading of soot to the boundary layer ranges from 1.5 to 20 $\mu\text{g m}^{-3}$ in urban areas⁸ to 0.2 to 2 $\mu\text{g m}^{-3}$ in rural areas.^{9,10} However, despite the fact that soot comprises less than 10% of the total aerosol mass in the atmosphere, its chemical and physical properties allows it to act as a precursor of gas-surface heterogeneous reactions, providing surface active sites for the reduction and oxidation of trace species in the atmosphere. Freshly emitted soot particles possess large porosities and significant internal surface areas, therefore having considerable high total aerosol fractal mass.¹¹ Its complex and varying chemical composition have been studied intensively in the past by different surface-sensitive techniques.¹²⁻¹⁴ Once emitted, soot mainly consist of 80-100% natural carbon, depending on the fuel; however a number of spectroscopic analysis of soot particles with Fourier Transform Infrared Spectroscopy (FTIR), Mass Spectrometer (MS) and X-ray Photoelectron Spectroscopy (XPS), between other techniques, have shown a wide range of functional groups from organic phases. Within the identified functional groups are hydroxyl, anhydride, carbonyl, carboxyl and other functional groups on its surface, indicating that soot composition is sensitive on the combustion conditions, fuel composition and oxygen/fuel mixing ratio.^{42,54} For example, a study by Kirchner et al. reported significant differences in the chemical composition of the particle surface of diesel soot and graphite-spark-generated soot with distinctly different mass spectra, showing different proportion of oxygen-containing carbonaceous fragments, minerals, and sulfur content in the particle surface.¹² In addition, in another study by Kirchner et

al. strong spectroscopic variations were shown to depend on the position in which the soot sample was collected with respect to the flame for hexane soot (top, center, and bottom of flame).¹⁵ In this respect, it is not surprising that the reactivity of soot toward heterogeneous reactions in the atmosphere can be different, according to the chemical's composition of the particles surface.

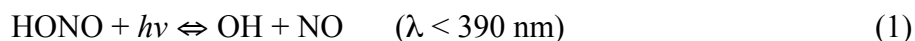
When freshly emitted to the atmosphere soot particles have a highly hydrophobic structure and can be easily oxidized in the atmosphere. As a consequence, soot particles can suffer many different functional group surface modifications through different processes by interacting with trace atmospheric species such as ozone,¹⁶⁻¹⁸ nitric acid,^{17,19} H_2SO_4 ,²⁰⁻²² between others. This is known as soot aging processes and it will depend on the environment where it is involved. For example, when soot is released in the atmosphere it can be oxidized by interacting with oxidizing atmospheric agents (e.i. ozone), increasing the oxygen-containing functional groups on its surface.¹⁶⁻¹⁸ Coagulation of soot particles with other pre-existing aerosols such as H_2SO_4 , HNO_3 , and organics acids²³⁻²⁶ are also possible in the atmosphere, altering its chemical reactivity or fate in the atmosphere. With this in mind, soot particles can play an important role by providing reactive sites where reductive reactions can take place in our highly oxidative atmosphere. An example of this is the heterogeneous reaction on soot aerosol surfaces, which attracted strong interest ever since Ammann et al. (1998) and Gerecke et al. (1998) found that significant amounts of HONO can be produced from the heterogeneous reaction of NO_2 with soot particles.^{27,28} In this way, soot certainly could

play an important role in changing the atmospheric chemical composition and have an impact on local or global weather, and human health.^{1-5,29,30}

1.2. Role of Nitrous Acid in the Urban Environments and the Reaction of NO₂ with Soot as Its Main Source

Nitrous acid (HNO₂), also referred as HONO in the literature, is the principal source of the most important daytime radical, the hydroxyl radical (OH). In many field measurements, the HONO concentrations have shown to increase during sunset and accumulate during the night in polluted urban environments.^{31,32} Field measurements made at Long Beach, California observed concentrations as high as 14 parts per billion (ppb) during the night; nonetheless, these concentrations rapidly decreased to concentrations lower than 1ppb as the sun rises.³¹ In rural and remote areas these concentrations are between 1 and 0.1 ppb, respectively.³²

The most important sink of HONO is photolysis (reaction 1). At sunrise, HONO concentrations drop because it is easily photolyzed by solar radiation, producing OH radicals and nitrogen monoxide (NO).³²⁻³⁴



This HONO cycle is the major source of OH radicals early in the morning when OH production rates from other sources are slow, potentially influencing the oxidation capacity of the atmosphere by enhancing photo-oxidation processes of volatile organic compounds whose reactions promote the formation of ozone and other secondary air pollutants.^{34,35} Therefore, HONO plays an important role in polluted urban environments.

Even though of its importance, the mechanism of formation of HONO is not yet completely understood and a number of sources have been proposed to explain the high HONO concentrations observed in polluted urban environments. Direct emissions from the exhaust of diesel vehicles, gas-phase chemistry, and heterogeneous aqueous chemistry of nitrogen oxides are some of the known sources of HONO that have been studied in laboratories and model calculations. Small HONO/NO_x ratios from 10⁻⁴ to 10⁻² have been measured from the exhaust of modern catalyst-equipped vehicles, which cannot explain by itself the high nighttime HONO concentrations measured in the boundary layer.^{37,38} HONO can also be produced via reaction of NO and OH radical (reverse reaction to equation 1), but this reaction is insignificant during the night because the OH concentration is very low.³⁸ A known source of HONO in laboratory systems is the NO₂ reaction with water adsorbed (reaction 2) on different surfaces:^{39,40}



However, reported HONO yields on soot exceeding 50% exclude this reaction with adsorbed water as the dominant process because the maximum theoretical HONO yield expected from this reaction is 50%. In addition, no investigation has detected the presence of nitric acid as a product of this reaction. As a consequence, a simplified oxidation-reduction process has been proposed, where NO₂ is reduced by hydrogen abstraction from the soot surface (R-H), producing HONO (reaction 3).



A wide range of NO₂ concentrations, temperatures, and a variety of carbonaceous materials—including commercial black carbon, different hydrocarbon flame soot, spark-

discharge soot, diesel soot, and power plant soot—have been used as soot aerosol models.^{15,41-46} The most widely used techniques for the uptake kinetics studies are the Knudsen reactor and the flow reactors coupled to a mass spectrometer using different ionization techniques. Most studies using different types of soot have shown a fast reactive uptake of NO₂ with the formation of HONO as the primary product. It has been shown that the reaction is non-catalytic since complete deactivation of soot has been observed.^{46,52} Other studies show regeneration of reactivity of soot by exposing it to water vapor^{41,44,53} and upon heating the soot sample.²⁸ As a consequence of the extensive studies carried out, a variety of HONO yields have been reported. For example, Longfellow et al. reported HONO yield as low as 13% on methane soot and 10% on propane soot at a low temperature of 262 K.⁴¹ However, Aubin et al. reported an average yield of 96% for hexane soot sample at ambient temperatures using similar NO₂ concentrations.⁴³ Aubin's results coincide with the work presented by Gerecke et al.,²⁸ Salgado and Rossi,⁵⁴ and Kleffmann et al.⁴⁵ Despite many studies, there is not a clear understanding of the heterogeneous reaction mechanism leading to the HONO formation and a significant discrepancy is present in the measured NO₂ kinetic uptake coefficients. As a result, there is a large uncertainty regarding the possible impact that the heterogeneous conversion of NO₂ to HONO on soot may have in polluted urban environments.

In laboratory studies, the sampling position on the flame has been shown to play an important role in the reactivity of soot toward NO₂. Gerecke et al. were the first to show that HONO yield decreases as soot is collected further away from a flame base

representing a more aged and oxidized soot with the percent of HONO yield varying from 93% at the base of the flame to 69% at the top of the flame.^{28,43} In addition, the combustion conditions have been shown to influence the reactivity of soot toward NO₂ and HONO production.^{15,42-45,55} Stadler and Rossi demonstrated that HONO yields of up to 100% can be measured from soot generated from a rich flame (high fuel/oxygen ratio), while the amount of HONO released from soot generated under lean flame (low fuel/oxygen ratio) conditions was very small.⁴² These observations suggest that the organic fraction that is condensed on the soot backbone may be involved in the HONO formation. Using (FTIR), Kirchner et al. found that the content of surface functional groups depend strongly on the soot type and sampling conditions.^{12,13,15,46,47} This adds an additional element to the experimental conditions with respect to the sample preparation in the attempt to explain the uncertainties in uptake kinetics and HONO yields.

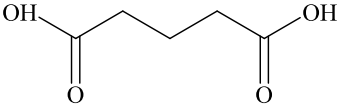
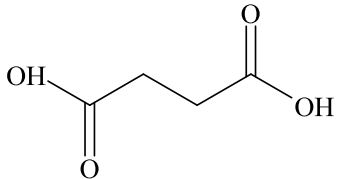
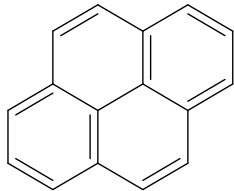
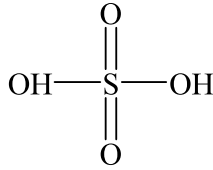
Different mechanisms for HONO formation have been proposed in order to explain the different behaviors observed for the heterogeneous conversion of NO₂ to HONO on soot for the different experimental conditions and sample preparation methods. The simplest mechanism involves the simple abstraction of a hydrogen atom from the soot surface (equation 2). An example of a more complicated mechanism involves the presence of a combination of competitive adsorption and reductive centers on the soot surface where NO₂ is converted into HONO.^{42,44,45} This last mechanism has been proposed in order to account for the reversible uptake of NO₂ on soot in addition to irreversible uptake.

In urban areas, the soot aerosol is of particular interest since its effects on global climate at short and long time scales are still uncertain.^{55,56} It is known that the oxidative aging of soot in the atmosphere occurs during its lifetime in the atmosphere (e.g. reaction with ozone) and these processes could significantly reduce its reactivity toward NO₂ and the HONO formation potential.^{15,41-44,47} The effect of soot aging on the NO₂ to HONO conversion potential has been studied by treating the soot sample with species such as ozone⁵⁶, nitric acid⁴⁵, and sulfuric acid⁴⁴, which are trace species commonly found in polluted environments. Soot samples treated with sulfuric and ozone before being exposed to NO₂ have shown significantly lower HONO yields.^{44,53} However, little is known about the effects of other soot aging processes, such as the internal mixing of soot aerosols with semi-volatile organic compounds. In addition, the mechanisms of reaction on soot surface toward HONO formation is still under debate in the literature. Some studies report that soot can be reactivated by pre-heating the soot sample²⁸ or in the presence of high relative humidity.^{41,44,53} While others argue that soot reacts with NO₂ irreversibly and its ability to generate HONO decreases after deactivation of all available reaction sites.⁴²⁻⁴⁴ These uncertainties need to be resolved in order to accurately predict the extent of HONO generation through heterogeneous reaction of NO₂ with soot using numerical models.

The study of the heterogeneous reaction of NO₂ on soot surfaces through a series of kinetic uptake experiments and HONO yield calculations was proposed by using Chemical Ionization Mass Spectrometry (CIMS) in an attempt to obtain a better understanding of the overall mechanism for the NO₂ uptake on soot leading to HONO

formation using an atmospheric-level NO_2 concentration of 5×10^9 to 5×10^{10} molecules cm^{-3} at 1.5 Torr, corresponding to atmospheric mixing ratios of about 0.2 to 2 ppb. The effect of atmospheric soot aging on the uptake coefficient of NO_2 and HONO yields after exposure of the soot surface to dicarboxylic acids (glutaric and succinic acids), sulfuric acid, and a polycyclic aromatic hydrocarbons (pyrene), was studied in order to gauge the potential effect of atmospheric aging processes. Table 1 shows the chemical formula, structure and molecular weight (MW) for each coating material. Soot samples were collected from the combustion of propane and kerosene fuels used as a model of atmospheric soot particles. The soot was deposited by either allowing the flame to touch the soot surface (Type A) similar to industrial channel black or by maintaining the deposition substrate (i.e. the soot surface) held high above the flame tip (Type B) as in lampblack processes. It is important to mention that when referring to Type A and Type B it is mainly to follow nomenclature convention used by Aubin and Abatt.⁴⁶ Characterization of the soot surface was carried out using Attenuated Total Reflection-Fourier Transmission Spectroscopy (ATR-FTIR) to examine the soot sample for the presence of different functional groups for fresh and aged soot after exposure of soot surface to the coating materials. A better understanding of the formation of HONO and its importance as a source of OH radicals is highly important for the improvement of air pollution models and possible future government decisions, regarding emission control strategies.

Table 1. Coating Materials

Name	Formula	MW (g mol ⁻¹)	Structure
Glutaric Acid	C ₅ H ₈ O ₄	132.12	
Succinic Acid	C ₄ H ₆ O ₄	118.09	
Pyrene	C ₁₆ H ₁₀	202.25	
Sulfuric Acid	H ₂ SO ₄	98.08	

2. EXPERIMENTAL

2.1. Preparation of Soot Samples

Freshly prepared soot samples were produced from the incomplete combustion of two hydrocarbon fuels—propane and kerosene. Gaseous propane was obtained commercially in a small gas cylinder tank. Liquid kerosene was obtained from the Alfa Aesar Company. The propane flame was generated using a commercial torch as a diffusion burner connected to the gas cylinder, while a commercial lamp chimney was used to maintain the kerosene flame. During the soot deposition process the flame was adjusted by altering the amount of fuel available to produce enough soot to speed up the soot deposition process (“sooting flame”). For every the air entrance was controlled by closing the space around the flame to avoid the fuel mixing with an excess of air before and during the combustion, keeping a stable diffusion flame. For kerosene combustion the wick length was adjusted at the beginning and the kerosene level inside the lantern is kept at high to obtain a stable and “sooting” flame. The flame soot was evenly deposited on the Pyrex glass tube inner walls with dimensions of 10 cm length and 1.6 cm inner diameter used as sample support.

The soot samples were prepared in two different deposition methods. The so-called Type A soot films were prepared by allowing the flame to touch the soot surface; whereas during, the preparation of Type B films the surface of soot was held high above the flame tip. Uniform soot coatings films were obtained by moving the sample support during the coating process. These methods will be referred to as Type A method and Type B method, respectively. The amount of soot flame generated with respect to time is

visibly different with these two deposition methods. With the Type B method the soot deposition process was faster than with the Type A method. For this reason, the Type B method was used to generate the soot samples for the soot-coating experiments described below.

The soot deposition processes for sample preparation varied from 3 to 20 minutes, depending on the amount of soot needed. The speed in which the mass of soot was deposited varied from fuel source to fuel source and between the two deposition methods. As expected, the propane combustion was more efficient, leading to slower soot deposition; while the kerosene combustion was less efficient, leading to faster soot deposition since more soot were generated with time. Soot produced with the two methods was visibly different in color. The Type A soot film was grey-like, while the Type B soot film was deep black. Typical soot sample masses ranging from 1 to 30 mg were collected and inserted in the flow reactor for the uptake kinetic experiments.

2.2. NO₂ Uptake and HONO Yield Measurements

The kinetic uptake experiments were carried out in a fast-flow, coated-wall reactor couple to a CIMS with a quadrupole mass analyzer shown schematically in Figure 1. The flow reactor (or flow tube) is a cylindrical Pyrex glass tube of 47 cm in length and internal diameter of 2.3 cm. A Pyrex glass tube (10 cm in length and with an inner diameter of 1.6 cm) with the soot-coated inner surface (soot sample) was inserted into the flow reactor, operated at typical flow rate of 50 to 200 sccm of dry helium carrier gas and at a low total pressure of 1.5 Torr at room temperature. Gaseous NO₂ was introduced as a continuous flow (steady-state experiments) into the reactor through a

central movable injector, which passed through the center from end to end of the soot-coated tube. Atmospherically relevant NO_2 concentrations of 5×10^9 to 5×10^{10} molecules cm^{-3} were used, corresponding to atmospheric mixing ratios of about 0.2 to 2 ppb.

Generally, every soot sample was exposed to dry helium gas for 15 to 20 minutes before being exposed to NO_2 , while stable background signals were reached. NO_2 with 21 ppm concentration, diluted in ultra-high pure helium, were prepared in a glass bulb and stocked in darkness. A fresh soot sample was used for every uptake experiment and the amount of soot on the glass tube was measured before and after each experiment.

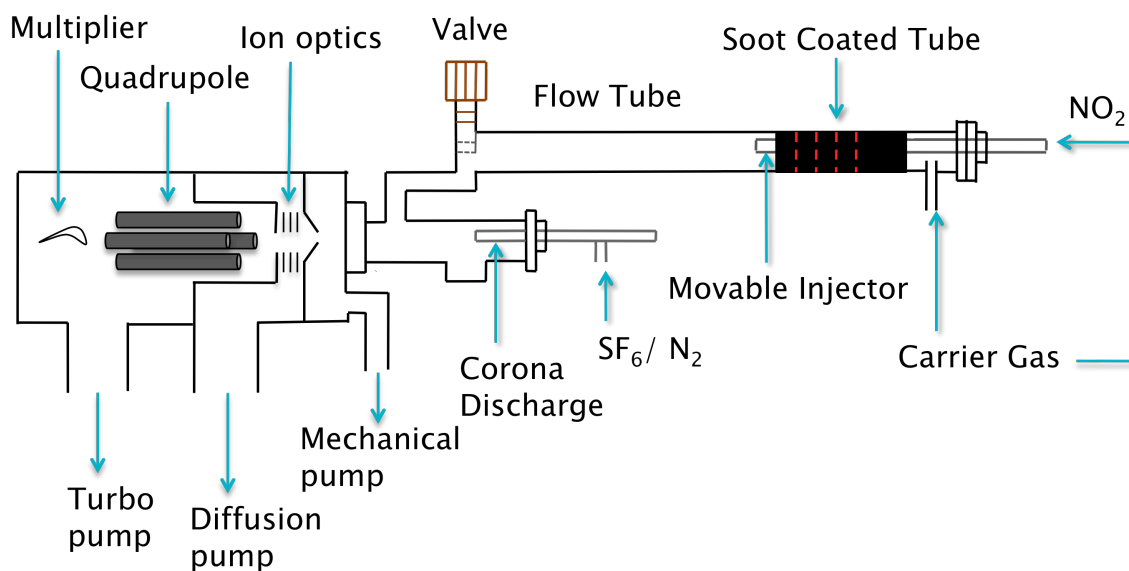


Figure 1. Diagram of the low-pressure fast flow reactor-CIMS system setup.

During the uptake experiments the reaction time varied by retracting the moveable injector to a position upstream of the soot tube (red dashed lines in Figure 1) by 2 cm increments exposing, the soot film to the NO₂ flow. After the exposure of the first 8 cm soot film the injector was pushed back to the starting position. The uptake of NO₂ and evolution of HONO were monitored by following the signals of nitrite (NO₂⁻; 46 m/z) and HF•NO₂⁻ (66 m/z) ions produced in ion–molecule reactions of NO₂ and HONO with the reagent ion SF₆⁻ (149 m/z):



The SF₆⁻ was produced by a custom-made corona discharge held at a high negative voltage in nitrogen carrier gas in the presence of 10 ppm SF₆. Previously measured rate coefficient for the electron-transfer reaction of SF₆⁻ to NO₂ (1.4x10⁻¹⁰ cm³ molecules⁻¹ s⁻¹) and for the fluoride ion-transfer reaction from SF₆⁻ to HONO (6x10⁻¹⁰ cm³ molecule⁻¹ s⁻¹) were used to calculate the NO₂ to HONO concentration ratio from the ratio of their mass spectrometer signals.⁴⁷ All metal gas lines and a gas purifier (oxygen trap) were implemented for oxygen-free (less than 50 ppb O₂) ion generation to minimize NO₂ background. All carrier flows were monitored with calibrated electronics mass flow meters (Millipore Tylan 260 Series) and all experiments were performed at (296 ± 2) K and a low total pressure of 1.5 Torr.

The uptake coefficient or reaction probability (γ) was determined by monitoring the NO₂ signal as it was exposed to the soot surface. It represents the ratio of the NO₂

molecules removed from the gas-phase to the total number of gas-surface collisions. The uptake coefficients, were calculated according to equation 6:⁴⁸⁻⁵⁰

$$\gamma = \frac{2rk_w}{\omega} \left[\frac{A_{geo}}{A_{BET}} \right] \quad (6)$$

where k_w is the wall-loss rate constant, r is the radius of the flow tube, ω is the mean thermal speed of NO_2 , A_{geo} is the geometric surface area of the soot inside the glass tube which was 50.26 cm^2 based on glass tube dimensions, and A_{BET} is the BET-surface area of the sample. BET stand for the authors: Brunauer—Emmett—and Teller, who developed the most common theory to determine the surface area of fine powders.⁵⁴

The asymptotic (irreversible uptake) part of the uptake curves was used to calculate the observed first-order rate coefficient (k_{obs}) for the NO_2 loss by plotting the natural logarithm of NO_2 signal versus the injector position. The wall-loss rate constant (k_w) was calculated from the k_{obs} for NO_2 loss by taking into account the diffusion rate constant of NO_2 in helium (k_d) from the center of the reactor to the wall:

$$\frac{1}{k_{obs}} = \frac{1}{k_d} + \frac{1}{k_w} \quad (7)$$

$$k_d = \frac{3.66 D_{P,He}}{r^2 P_{He}} \quad (8)$$

where $D_{P,He}$ is the diffusion coefficient of NO_2 in helium at pressure P_{He} . Control experiments, using CIMS, conducted on bare Pyrex tubes showed no uptake of NO_2 or formation of HONO.

HONO yield measurements, relative NO₂ loss, were calculated from the heterogeneous reaction of NO₂ with soot. The yields of HONO were determined as a ratio of the number of HONO molecules released (i.e. produced by the reaction) to the number of NO₂ molecules taken up, on kerosene and propane soot, during the same exposure time. Both NO₂ and HONO signals were corrected with respect to the background signals. The amount of NO₂ loss to the soot surface and HONO molecules released, after the retraction of the injector, were determined by integration of the loss and gain of signals, respectively. Control experiments were conducted on a bare Pyrex tube (blank sample), and no uptake of NO₂ and formation of HONO were observed.

The reactivity of soot (i.e., NO₂ uptake coefficient or reaction probability) toward NO₂ was also studied for pre-heated soot samples. After fresh soot samples were analyzed, the same sample were pre-heated to 300 °C in vacuum for 30 minutes and immediately analyzed again in the flow reactor to see the effect in the soot kinetics for NO₂ in terms of uptake coefficient and yield of HONO.

2.3. Soot Coating with Different Vapors

The effect of soot coating (atmospheric “aging” effect) on the reactivity of soot was also studied. The soot coating procedures were done in two different ways, inside the flow reactor (*in situ*) and externally to the reactor. The fresh soot samples were exposed to succinic acid (Sigma-Aldrich, 99%), glutaric acid (Sigma, 99%), sulfuric acid (Sigma-Aldrich, 96%), and pyrene (Aldrich, 98%), shows in Table 1. In the first approach, a sample bubbler containing the acid was placed in a temperature bath to regulate its concentration in the flow reactor. The acid vapor was introduced through the

movable injector and the coating progress was monitored by following the concentration of the gas-phase species in the flow reactor. The detection of organic acids and sulfuric acids (RH) was accomplished using CIMS with either SF_6^- or CO_3^- reagent ions:



ATR-FTIR spectra were taken (described in section 2.2) to the coated-soot sample at different locations inside the glass tube (top, middle and bottom part) and very small amount of coating material (based on the characteristics features peaks) were achieved by the *in situs* coating approach. In fact, the ATR-FTIR spectra showed the coating was not uniform throughout the soot surface and no effects were observed in the soot reactivity toward NO_2 and HONO yield.

Thicker coatings were produced by inserting the soot-coated glass tubes inside an evacuated glass container with a sample of the coating material at the bottom (Figure 2). Just the bottom part of the glass container was heated without heating the soot sample and small helium flow was set inside to help distribute the coating material more uniformly throughout the soot surface. A heating tape, controlled by a Variac voltage transformer was set at different temperatures, according to the vapor pressure of the coating material in order to coat the soot. For glutaric acid the temperature was set to 85 °C, for succinic acid temperature was set to 100 °C, for pyrene it was set to 90 °C and for sulfuric acid temperature was set to 85 °C approximately. This soot-coating procedure was carried out for 30 minutes for each soot sample. ATR-FTIR spectra showed better soot coating all around the soot surface but not uniform. This coating

procedure was applied to all fresh unactivated soot samples through a complete series of continued experiments. After the fresh soot samples were analyzed, the samples were then treated with either of the coating materials and immediately analyzed in the flow reactor for NO₂ uptake and HONO yield. Control experiments performed on fresh soot samples showed that uptake coefficients were reproducible from consecutive NO₂ uptake experiments carried out to the same soot sample. In addition, control experiments performed on bare Pyrex tubes coated with each vapors material showed no uptake for NO₂ and HONO formation during uptake experiments.

2.4. Soot Characterization by ATR-FTIR Spectroscopy

Attenuated total reflection fourier transform infrared spectrometer (ATR-FTIR) was used to analyze the chemical composition of both Type A and Type B kerosene and propane soot samples before (fresh sample) and after pre-heating to 300 °C. Knowledge of the soot surface functional groups and structure could provide us information about the reaction mechanism of NO₂ with soot. ATR-FTIR spectra of the Type B kerosene and propane soot samples before and after the exposure to the coating materials were also taken to confirm the presence of the coating material on the soot surface.

The ATR-FTIR instrument used in this study was a Perkin Elmer Spectrum 100 employing a MIR TGS detector. The crystal type used was zinc selenide (ZnSe) mounted in a flat plate. The crystal had a trapezoid shape with dimensions of 80 mm long, 10 mm wide, 4 mm thick, and a penetration depth of 0.5μ to 5μ. Background scan, with no sample on the face of the crystal, were collected before sample spectrum were collected. The ATR spectrum of the required samples were obtained by rationing a

sample scan collected to the background scan and corrected for comparison to FTIR spectra after averaging a collection of 64 scans at resolution of 4 cm^{-1} over the typical wavenumber range from 4000 to 750 cm^{-1} . The soot sample was deposited over a commercial aluminum foil, which was molding the inner surface of the glass tubes, following the ways described above. The foil was removed from the glass tube and three strands were cut at the top, middle and bottom parts relative to its positions over the flame or its position relative to the coating material in the container. Since the ATR effect takes place at the surface of the crystal, the strands were cut to fit into the flat plate press, above the ATR crystal, allowing efficient contact between the sample and the crystal surface. The ATR crystal was cleaned between experiments to avoid cross contamination. Blank samples confirmed the absence of contamination on the ATR crystal before the soot sample was placed for analysis on each experiment.

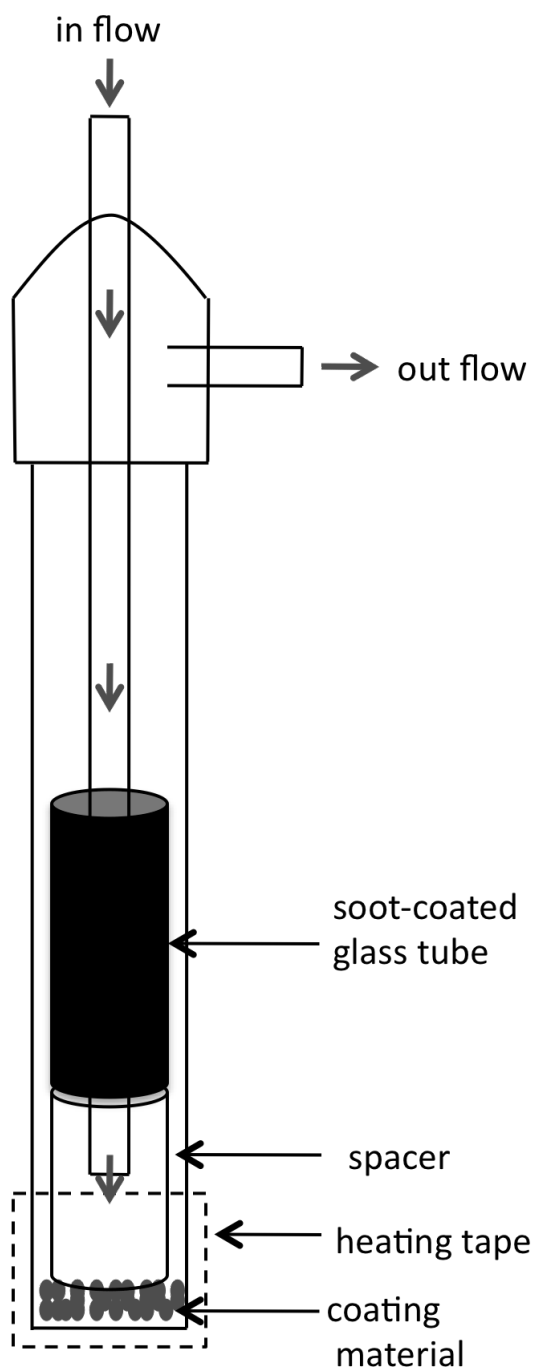


Figure 2. Diagram of the evacuated glass container where soot was coated.

3. RESULTS AND DISCUSSION

3.1. NO₂ Uptake and HONO Yields on Different Types of Soot

NO₂ uptake measurements were performed by exposing the soot film to NO₂ while monitoring the signals of NO₂ and HONO with CIMS. The injector was retracted, beginning with 2 cm up to 8 cm length in 2 cm increments inside the soot-coated tube for 3 to 5 minutes approximately, exposing the soot film to the NO₂ flow. NO₂ concentrations, ranging from 5×10^9 to 5×10^{10} molecules cm⁻³ at 1.5 Torr were used, equivalent to atmospheric mixing ratios of about 0.2 to 2 ppb.

Typical temporal profiles for NO₂ uptake and HONO formation on Type A and Type B fresh (unheated) soot films from the incomplete combustion of kerosene and propane fuels are shown in Figure 3 and Figure 4. A large and fast NO₂ uptake was observed when the soot sample was initially exposed (first 2 cm) to the NO₂ flow at approximately 220 s, indicative of the NO₂ partitioning to the soot surface. Unheated kerosene soot samples, whether Type A (Figure 3a) or Type B (Figure 3b), showed a combination of reversible and irreversible uptake. The reversible uptake is represented by a slow asymptotic recovery after the fast uptake of NO₂. The slow asymptotic recovery indicates NO₂ molecules leaving the soot surface and thus increasing the NO₂ gas-phase concentration. The irreversible part was reached when the NO₂ signal attained a constant level after the exposure. Simultaneously to the uptake of NO₂, an increase in the HONO signal was observed. This shows that the conversion of NO₂ to HONO on soot surfaces is a fast process. The HONO signal also decreased asymptotically, but remained above zero on the time scale of the experiments.

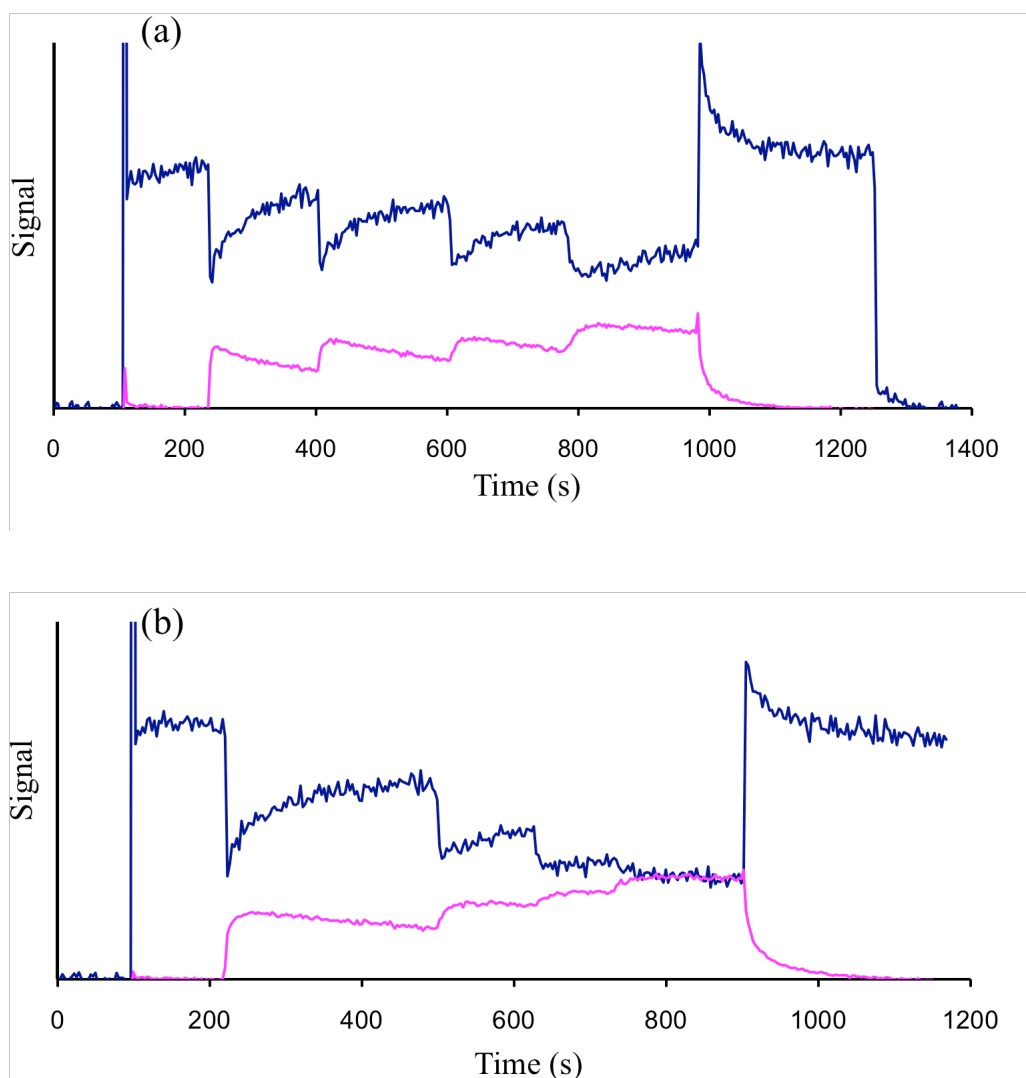


Figure 3. Temporal profile of NO_2 uptake and HONO production on Type A (a) and Type B (b) fresh kerosene soot with stepwise exposure in 2 cm increments up to 8 cm in length of 5 and 10 mg of soot respectively. Experimental conditions were $T = 298 \text{ K}$, $P = 1.5 \text{ Torr}$, $U = 134 \text{ cm s}^{-1}$ and $[\text{NO}_2] = 1 \times 10^{10} \text{ molecules cm}^{-3}$. The injector was returned to its original position after $\sim 1000 \text{ s}$ for plot (a) and 900 s for plot (b).

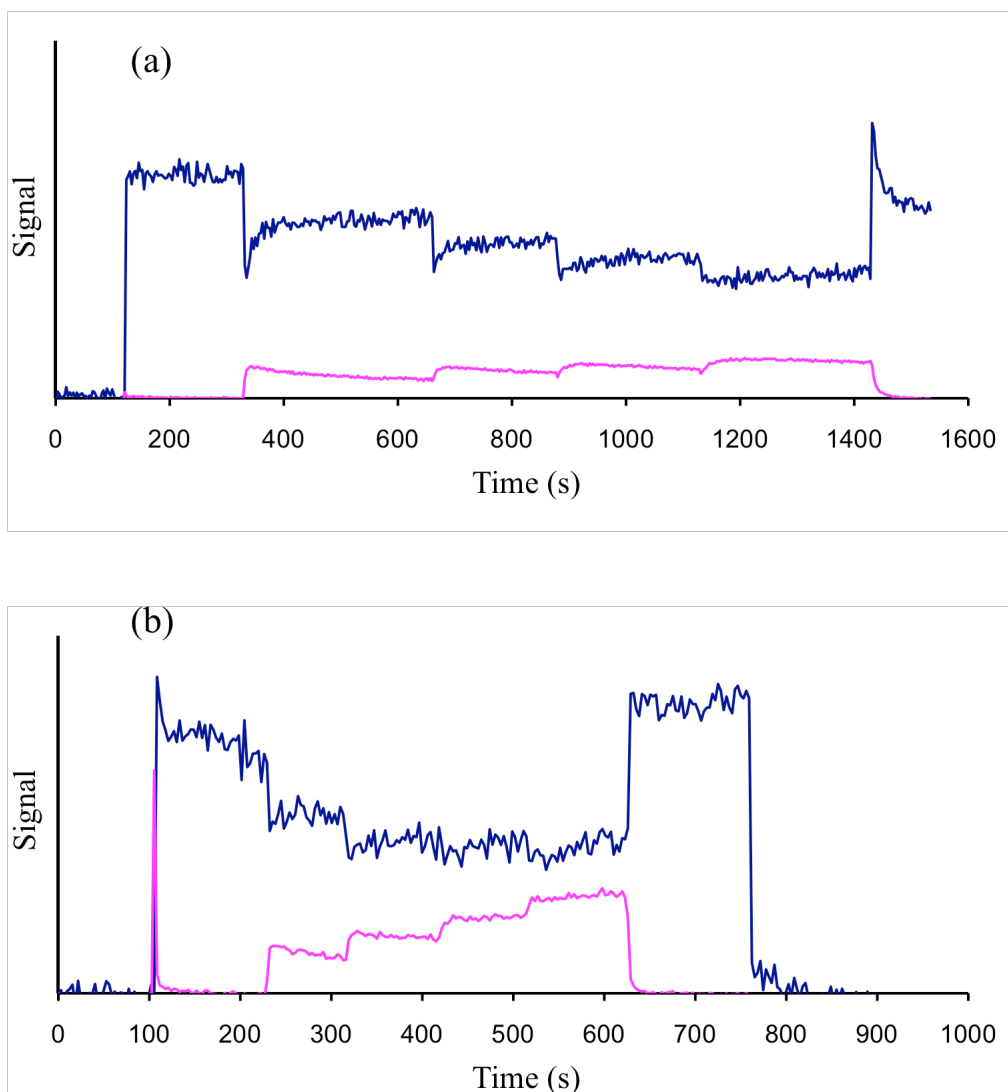


Figure 4. Temporal profile of NO₂ uptake and HONO production on Type A (a) and Type B (b) fresh propane soot with stepwise exposure in 2 cm increments up to 8 cm in length of 16 and 7 mg of soot respectively. Experimental conditions were $T = 298 \text{ K}$, $P = 1.5 \text{ Torr}$, $U = 134 \text{ cm s}^{-1}$ and $[\text{NO}_2] = 1 \times 10^{10} \text{ molecules cm}^{-3}$. The injector was returned to its original position after 1400 s for plot (a) and 600 s for plot (b).

As shown in Figure 3, the decrease in NO_2 uptake correlates with the rate of HONO formation. By withdrawing the injector for a total of 8 cm in length over the soot film an uptake pattern with progressively lower asymptotic NO_2 signal and less distinct reversible parts at longer reaction time is obtained (Figures 3 and 4). When the injector was pushed downstream to the original position, approximately at 1000 s (Figure 3a), a complete recovery of the signal was observed. Less than half of the NO_2 that was taken up came off the surface. The experiments with the Type A propane soot, Figure 4a, showed a shorter and less pronounced reversible part of the NO_2 uptake when compared with kerosene soot samples. In the case of Type B propane soot, only the irreversible part was observed, Figure 4b, and when the interaction between NO_2 and soot was stopped, by pushing the injector back to initial position, no NO_2 came off the soot surface. The profiles shown in Figures 3 and 4 are typical of soot for the two types of fuels used, and such profiles are the basis of all the experimental results presented in this study.

After kinetic uptake experiment for the fresh soot sample was done, the sample was heated at 300 °C in vacuum for 30 minutes. Then the kinetic uptake experiment was repeated for the pre-heated soot sample. Figure 5 shows NO_2 uptake and HONO production on a Type A pre-heated soot sample. Pre-heating the soot sample causes drastic increases in the reactivity of soot leading to substantial HONO formation and HONO signal to remain constant during the time scale of the experiments. It did not matter what type of fuel or flame regime was used during the soot film preparation, the NO_2 uptake on heated soot samples was practically irreversible and leads to higher

HONO production. In addition, a significant initial drop of NO₂ signal in each pre-heated soot sample for the first 2 cm of the soot film exposed to the NO₂ flow and a corresponding significant increase in HONO signal were observed simultaneously. However, small additional NO₂ uptake and HONO production were observed when additional soot surface was progressively being exposed to the NO₂ flow by retracting the injector. This occurs because heterogeneous interaction becomes limited by gas-phase diffusion since the heterogeneous NO₂ loss becomes much more efficient, leading significant depletion of NO₂ near the soot surface. As a consequence, the NO₂ diffusion from the volume toward the soot surface became rate-limiting in the heterogeneous reaction under our experimental conditions and time scale of the experiment for pre-heated soot samples.

The observed effect of heating on the reactivity of soot can be interpreted by the removal of volatile organic soot fraction. Heating the soot sample causes the removal of organic condensed matter, unblocking surface-active centers that were occupied before and making them accessible for reaction with NO₂. Incomplete combustion of hydrocarbon fuels is known to produce semi-volatile organic compounds, mainly polycyclic aromatic hydrocarbons (PAH), which condense on soot upon cooling.⁵⁸ The fraction of volatile material produced in the flame increases with the flame equivalence ratio and, for the diffusion flame used in our study, with molecular weight (or C/H ratio) of the hydrocarbon fuel. From the NO₂ temporal profiles, shown in Figures 3 and 4, we can clearly identify a pattern; that in the sequence Type A kerosene soot – Type B kerosene soot – Type A propane soot – Type B propane soot, the contribution from the

reversible uptake progressively decreases while irreversible uptake becomes dominating because kerosene produces richer flame than propane, leading to more condensable matter. The removal of the semi-volatile components during heating of soot samples under vacuum to 300 °C was confirmed by direct observations. After heating several kerosene soot samples a brownish thin film gradually built up on the cooler top part of the glass container. The film was less visible for propane soot samples, which carries lower fraction of condensed organic matter. For both kerosene and propane soot, the heating did not cause an observable sample mass changes (i.e., the change is less than 2% of the sample mass). Also, no change in the infrared spectra of soot was observed after heating (Figure 6), indicating that the mass of the condensed matter was relatively small.

HONO yields defined as the ratio of the number of HONO molecules produced for every NO₂ molecules taken up, on kerosene and propane soot, during the same exposure time for the heterogeneous interaction of NO₂ with the different types of soot are summarized in Figure 7 for fresh soot samples. Type A soot samples produce the highest yield, approaching 100% specifically for the soot samples with small mass. As the sample mass increases, less HONO is produced per each molecule of NO₂ taken with yields as low as 6% calculated for a 13 mg Type B propane soot sample. Substantial variation in HONO yields for samples of the same mass was observed, which can be attributed to variations in the flame conditions such as fuel/oxygen ratio, flame stability, flame length and air turbulence around the flame, that may have happened during the preparation from one sample to another. Variation in combustion conditions lead to

variable amount of condensed organics produced from the flame. In addition, it can lead to soot morphology changes and variations in the soot film thickness across the glass substrate (glass tube). However, as shown in Figure 8, the effect of pre-heating the soot samples before exposing the sample to NO_2 showed better reproducibility on the HONO yields for the different types of soot. The large majority of the pre-heated soot samples showed HONO yields above 50% and the trend of decreasing HONO yield as the soot mass increases was observed. In addition, less difference in soot HONO yields was observed between different types of samples for pre-heated soot, compared with fresh ones. A comparison between Figures 7 and 8 shows that heating the soot samples increases HONO production, especially for Type B soot samples. This indicates that even small amounts of condensed organic matter on freshly emitted soot can have an effect on its HONO production capability.

The NO_2 signal drop by retracting the injector was plotted against the injector position (reaction time) for each uptake experiments by using the asymptotic (irreversible) part of the uptake curves, as shown in Figures 3 and 4. Figure 9a shows typical NO_2 signal decay as a function of injector position for 2 mg of Type B kerosene soot sample, both fresh and pre-heated. The experiments were conducted at a 1.5 Torr total pressure, total flow of 134 cm s^{-1} and NO_2 concentration of $1 \times 10^{10} \text{ molecules cm}^{-3}$. The decay follows first-order kinetics and linear regression analysis of each data set was performed to obtain the observed first-order rate coefficients k_{obs} , which was used to calculate the NO_2 uptake coefficients, as described in section 2.2. The ratio of geometric surface area to BET-surface area was used as shown in equation 3. BET-surface area of

the soot samples were calculated using the sample mass together with BET-specific surface area for different soot types previously measured in our laboratory (Levitt et al.)⁵⁹ as shown in Table 2.

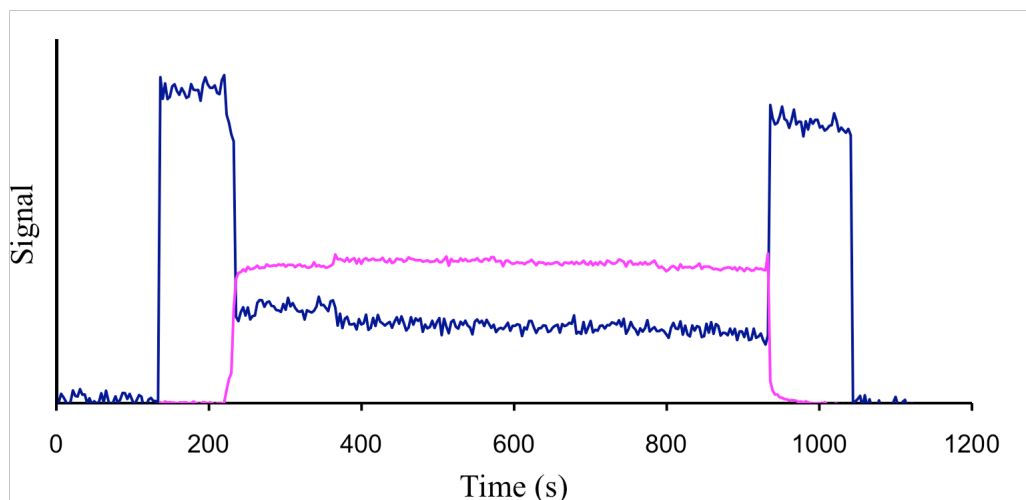


Figure 5. Temporal profile of NO_2 uptake and HONO production on 16 mg of pre-heated Type A propane soot with stepwise exposure in 2 cm increments up to 8 cm in length. This sample was pre-heated at $T = 300\text{ }^\circ\text{C}$ in vacuum for $t = 30$ minutes. The experimental conditions were $T = 298\text{ K}$, $P = 1.5\text{ Torr}$, $U = 134\text{ cm s}^{-1}$ and $[\text{NO}_2] = 1 \times 10^{10}\text{ molecules cm}^{-3}$. The injector was returned to its original position after 900 s.

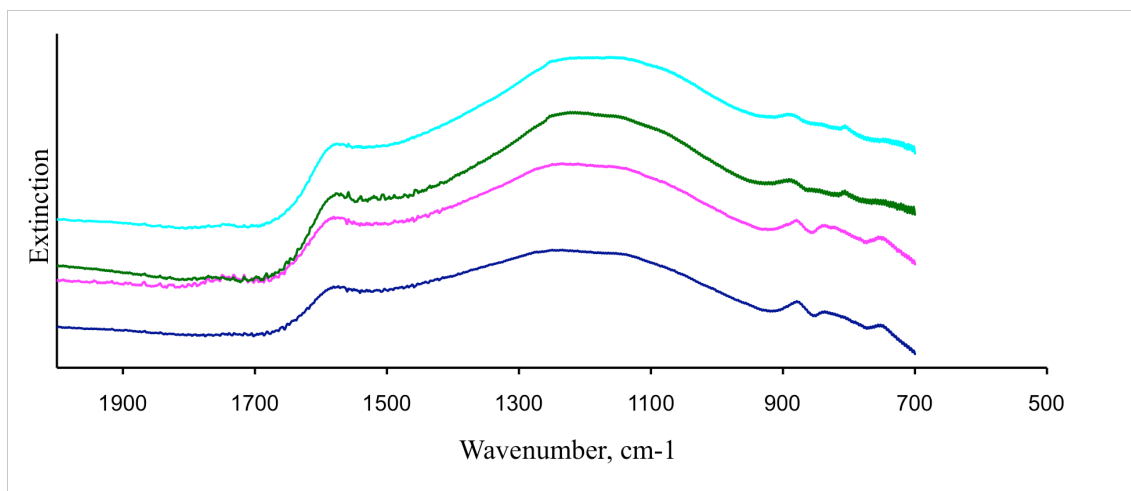


Figure 6. ATR-FTIR spectra of Type A and Type B propane soot deposited on a ZnSe crystal plate, before and after heating the soot sample to 300 °C in vacuum for 30 min. The top two spectra are Type A samples fresh and pre-heated respectively, while the bottom two are Type B fresh and pre-heated samples respectively. The spectra were offset along the ordinate for clarity.

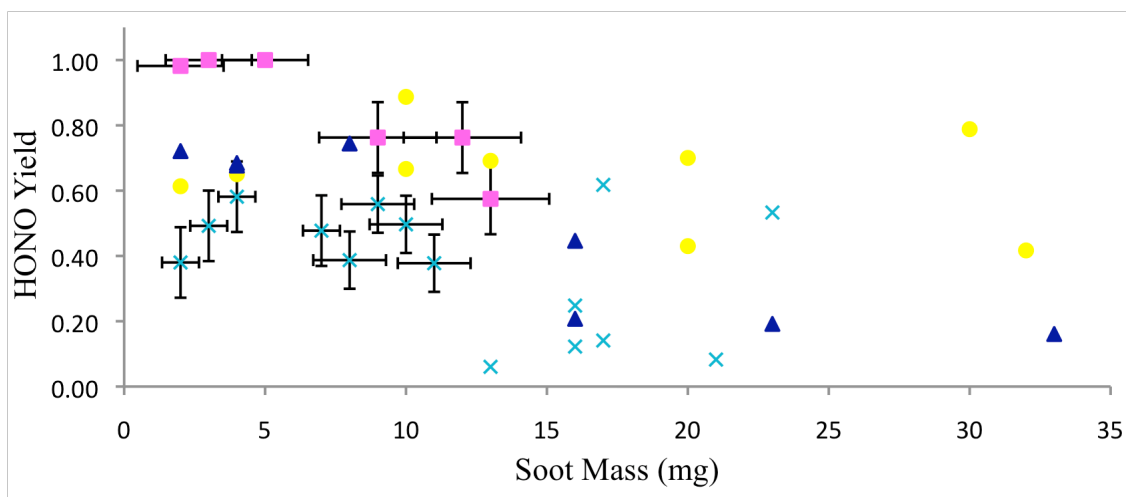


Figure 7. Summary of HONO yields determined from the heterogeneous reaction of NO_2 with fresh Type A kerosene soot (square), Type A propane soot (triangle), Type B kerosene soot (circle), and Type B propane soot (cross) as a function of soot mass. NO_2 concentration was 1×10^{10} molecules cm^{-3} .

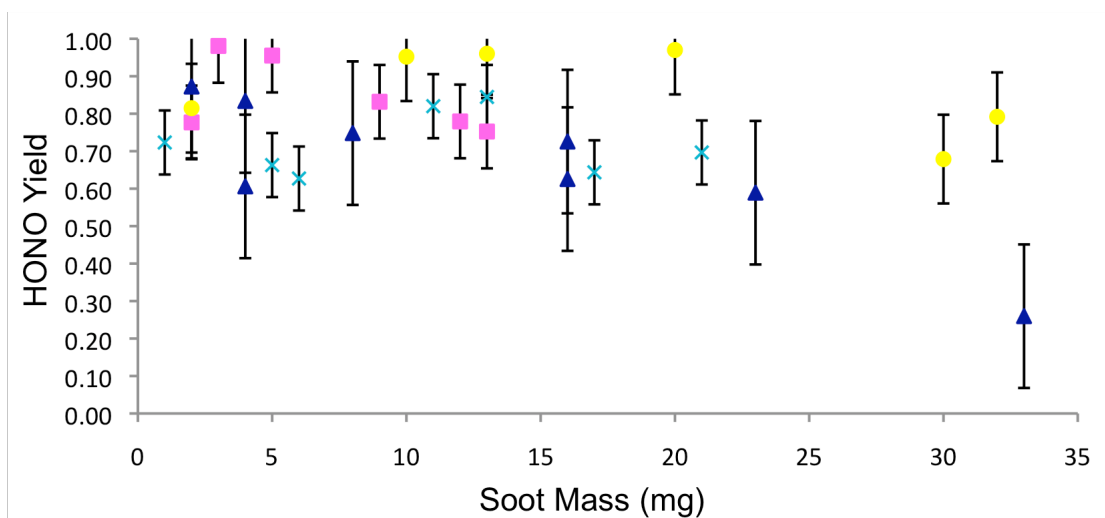


Figure 8. Summary of HONO yields determined from heterogeneous reaction of NO_2 with pre-heated Type A kerosene soot (square), Type A propane soot (triangle), Type B kerosene soot (circle), and Type B propane soot (cross) as a function of soot mass. NO_2 concentration was 1×10^{10} molecules cm^{-3} .

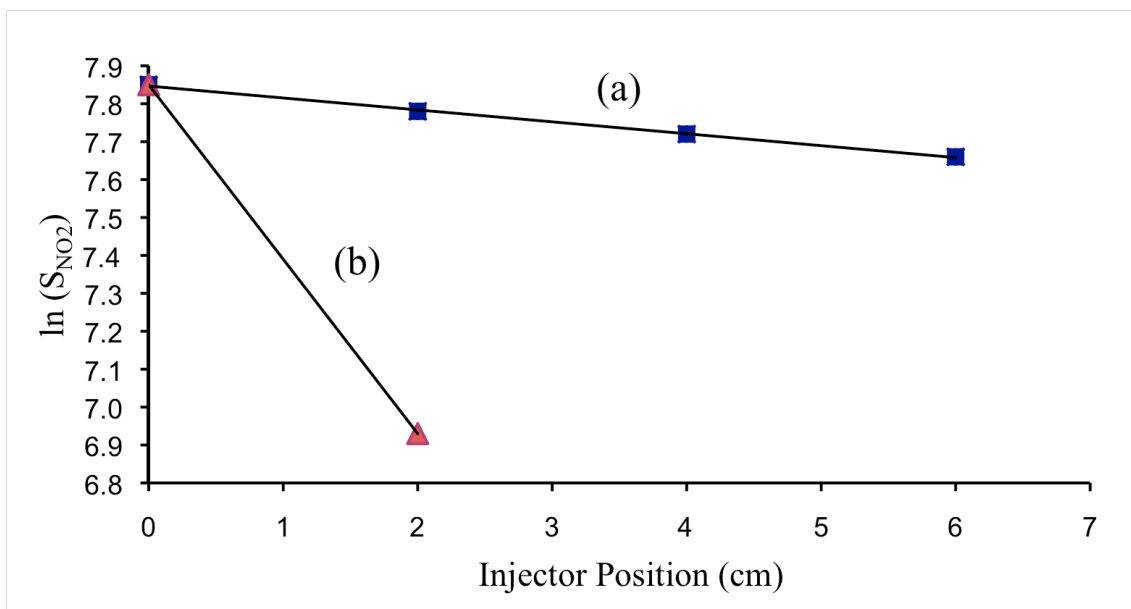


Figure 9. Natural log of NO_2^- signal as a function of injector position on 9 mg of Type B kerosene soot sample, fresh (a) and pre-heated to 300 °C for 30 min in vacuum (b). The experimental conditions were $T = 298 \text{ K}$, $P = 1.5 \text{ Torr}$, $U = 134 \text{ cm s}^{-1}$ and $[\text{NO}_2] = 1 \times 10^{10} \text{ molecules cm}^{-3}$. The observed rate constant (k_{obs}) was obtained from the slope of the linear regression.

Table 2. Summary of BET Specific Surface Areas^a

Fuel	BET specific surface area, $\text{m}^2 \text{ g}^{-1}$	
	Type B	Type A
Propane	$146.95^{\text{b}} \pm 18.29^{\text{c}}$	78.45 ± 24.92
Kerosene	105.5 ± 18.70	66.57 ± 13.08

^a Data was obtained from Levitt et al.⁵⁹

^b Average value of soot samples with different masses

^c Error corresponds to second standard deviation (2σ)

Figure 10 shows the kinetic uptake coefficients for the heterogeneous interaction of NO₂ with the different types of soot, including fresh and pre-heated, as a function of the soot sample mass. The uptake coefficients of NO₂ for the different types of soot varies from 5.6×10^{-6} to 1.6×10^{-4} for fresh soot samples, and from 3.0×10^{-5} to 4.4×10^{-4} for pre-heated soot samples, both decreasing with the soot sample mass. This decreasing trend might have been caused by NO₂ not being able to reach deeper layers of soot on the time scale of our experiments. Therefore, it is possible that not all BET sample surface is being probed for the heterogeneous reaction. Our NO₂ uptake coefficients for fresh soot samples compare with those measured by Lelievre et al. (4.0×10^{-5} on kerosene soot)⁵², Kleffmann et al. (10^{-6} on carbon black)⁴⁵, and Aubin and Abbatt (3.9×10^{-5} on hexane, decane and benzene soot)⁴³ using BET-surface area of soot.

Figure 10 also shows that pre-heating soot samples before the uptake experiments lead to a significant increase in the uptake rate coefficient. It is important to mention, as shown in Figure 9b, that for the majority of the pre-heated soot samples only two points in the regression line could be plotted since no additional NO₂ loss was observed after retracting the injector beyond 2 cm length of soot film. This is indicative, as explained above for Figure 5, of gas-phase diffusion limitation since the heterogeneous NO₂ loss became much more efficient, leading to fast depletion of the local NO₂ molecules close to the surface. As a consequence, the NO₂ diffusion from the volume toward the soot surface becomes rate-limiting in the heterogeneous reaction for pre-heated samples under our experimental conditions and time scale of the experiments. Therefore, the uptake coefficients calculated for pre-heated soot samples in this work

represent a lower limit of actual values. However, it is also possible that heating the soot sample led to an increase of the soot surface area, in such case would lead to an overestimation of our uptake coefficients since we assumed that the soot surface did not change after heating.

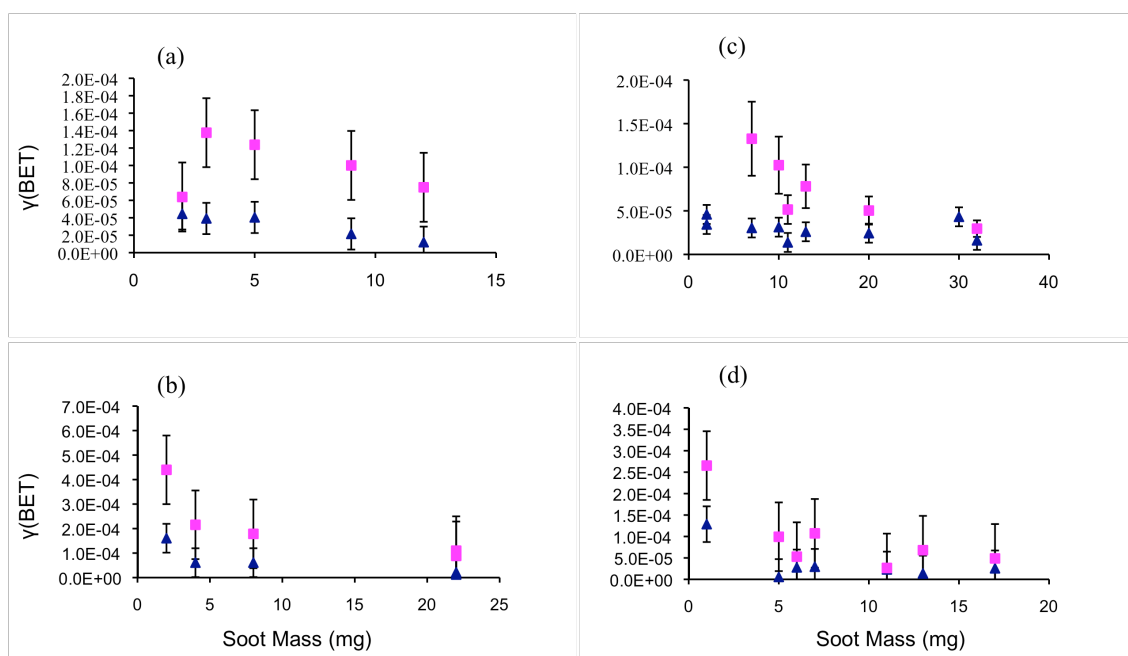
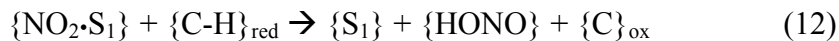


Figure 10. NO₂ uptake coefficients for fresh (triangle) and preheated (square) soot as a function of soot mass for the different types of soot including Type A kerosene soot (a), Type A propane soot (b), Type B kerosene soot (c), and Type B propane soot. The experimental conditions were $T = 298 \text{ K}$, $P = 1.5 \text{ Torr}$, $U = 134 \text{ cm s}^{-1}$ and $[\text{NO}_2] = 1 \times 10^{10} \text{ molecules cm}^{-3}$ with the same experimental time scale.

3.2. Mechanism of NO₂ Uptake and HONO Production

Yields over 50% discard the surface-catalyzed disproportionation reaction in the presence of adsorbed water as the dominant process for HONO production since the maximum theoretical HONO yield expected from this reaction is of 50% (equation 2).

High yields observed in our study are consistent with an alternative reduction-oxidation mechanism proposed by Gerecke et al.²⁸ and further developed by Stadler and Rossi⁴² and Aubin and Abbatt.⁴³ The mechanism can be described by the following processes:



The species in brackets refer to surface adsorbates. In equation 11, the initial uptake of NO_2 occurs, where the NO_2 molecule interacts with the soot surface adsorption site $\{\text{S}_1\}$, leading to $\{\text{NO}_2 \cdot \text{S}_1\}$. This interaction is probably weak, allowing for the NO_2 molecules enough mobility to reach the reducing surface site, represented in equation 12 as $\{\text{C-H}\}_{\text{red}}$. Equation 11 corresponds to the observed reversible part of the uptake curves shown in Figures 3 and 4. Equation 12 represents the second step, where a chemical interaction between the adsorbed NO_2 molecule, in the form of $\{\text{NO}_2 \cdot \text{S}_1\}$, and the surface site $\{\text{C-H}\}_{\text{red}}$ occurs. The $\{\text{C-H}\}_{\text{red}}$ sites reduce the NO_2 molecule, leading to nitrous acid adsorbed in the soot surface, $\{\text{HONO}\}$, and the site becomes oxidized $\{\text{C}\}_{\text{ox}}$. The active site $\{\text{C-H}\}_{\text{red}}$ in the second step is providing the hydrogen for the heterogeneous NO_2 reduction to HONO, such as allylic hydrogen atoms on the soot surface as have been suggested by Aubin and Abbatt⁴³ and Stadler and Rossi.⁴² Therefore, soot is considered in this mechanism as a reactant rather than a catalyst, where its active sites are consumed.

The rapid initial drop in NO_2 uptake and HONO formation rates (reversible part of the uptake curves shown in Figures 3 and 4) are caused by a temporary depletion of the surface adsorption sites $\{\text{S}_1\}$. In the fresh soot samples, some of these surface

adsorption sites are blocked by the condensed organic matter. Based on our results and judging by this mechanism the physical adsorption on these sites is a limiting step for the heterogeneous NO₂ to HONO conversion on soot, which explains why the significant changes in the reactive and kinetic behavior of fresh and pre-heated soot samples toward NO₂ were observed. Heating the soot sample released condensed volatile organic matter from the soot backbone, unblocking many of these adsorption sites, resulting in chemical reaction (equation 12) as a limiting step and hence irreversible NO₂ uptake. This is the reason for the observed reactivation of soot previously exposed to NO₂ by heating, but at lower yields reported by Gerecke et al.²⁸ However, no re-activation of the previously exposed NO₂ samples was observed upon exposure to 50% relative humidity of the ambient air. In addition, soot samples left for several days after preparation gradually decreased their ability to generate HONO that may be explained by trace amounts (few ppb) of NO₂ present in the ambient air reacting with the soot sample. The deactivation of soot in ambient air with time is another proof that the heterogeneous reaction of NO₂ on soot leading to HONO formation is not a catalytic process.

HONO formed in the second step (equation 12) can either desorb from the surface to the gas-phase, giving rise to the observed mass spectrometer HONO-signal (equation 13), or react on the surface producing NO and NO₂ (equation 14). Disproportionation of adsorbed HONO on the soot surface as well as the reaction of NO₂ with surface sites of another kind (equation 15) may explain HONO yields below 100%.





In summary, the yield of HONO seems to depend on the competition between processes 11-12, and 14-15. Heating the soot unblocks more $\{\text{S}_1\}$ adsorption sites, promoting processes 11 and 12 to lead to higher HONO yields. It is possible that heating the soot sample causes a change in the BET-surface area as well, however it was not tested. Based on this proposed mechanism, the effect of soot “aging” on the reactivity of soot toward NO_2 and HONO production will depend on the binding location of the condensing species in the soot backbone. The yields of HONO may decrease or increase depending on whether sites $\{\text{S}_1\}$ or $\{\text{S}_2\}$ are preferentially occupied.

3.3. Effect of Coated Soot on the NO_2 Uptake Coefficients and HONO Yields

The soot coating procedure was first carried out inside the flow reactor (*in situ*) using the sample bubbler that contained the condensing material (H_2SO_4 , glutaric acid, succinic acid, and pyrene) placed in a temperature bath to regulate the concentration of vapors in the flow reactor. The vapor was introduced through the movable injector in helium carrier gas, and the coating progress was monitored by following the concentration of the gas-phase vapor using CIMS, as described in section 2.3. Figure 11 demonstrates the uptake of glutaric acid on 4 mg of Type A kerosene soot. The exposure of soot to low concentrations ($\sim 10^{11}$ molecule cm^{-3}) of glutaric acid vapor started at 4800 s and ended at 7300 s. As displayed in Figure 11, glutaric acid showed a reversible uptake (Levitt et al.)⁵⁹ on Type A kerosene soot, consisting of fast and slow regions, corresponding to different active sites or penetration depth. This exposure results in a surface coverage lower than 0.1% and subsequent measurements of NO_2 uptake on this

soot sample showed no effect of small glutaric acid coating on the NO_2 uptake coefficient (reaction probability) or HONO yields.

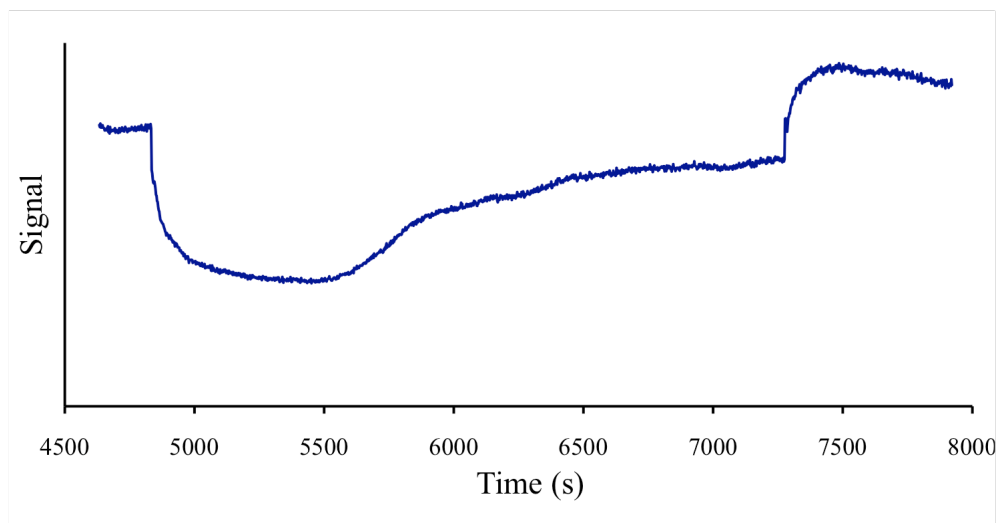


Figure 11. Temporal profile of glutaric acid with temporary exposure to 4 mg of Type A kerosene soot over 8 cm in length. The exposure started at 4800 s and ended at 7300 s.

Larger coatings were achieved by inserting the soot-coated glass tubes inside an external evacuated glass container with a small sample of the coating material at the bottom, Figure 2. The bottom part was heated with the soot sample kept at room temperature, while a small helium flow was set inside to help distribute the coating material more uniformly throughout the soot surface. This soot-coating procedure was carried out for 30 minutes for each soot sample at specific temperatures (section 2.3). A limitation of this external coating method is due to the fact that the exact amount of coating material deposited (surface coverage) on the soot surface cannot be calculated. Although no measurable sample mass increase was observed after coating, the presence

of glutaric acid on soot was confirmed by ATR-FTIR as shown in Figure 12, comparing the spectra of Type B kerosene soot before and after exposure to glutaric acid vapor with the spectrum of pure glutaric acid and the corresponding spectrum for the fresh soot. Although, larger soot coating on the soot surface was achieved the coating was not uniform since the coated soot spectra at different location (top, middle, and bottom), with respect to the sample position in the container, showed that more coating material was deposited on the side closer to the coating material (bottom part).

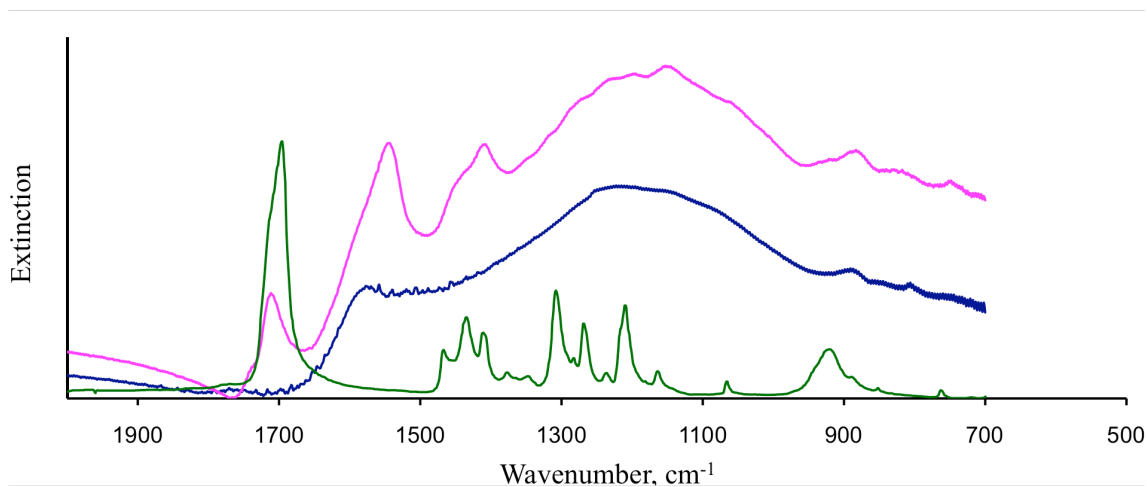


Figure 12. ATR-FTIR spectra of Type B kerosene soot deposited on a ZnSe crystal plate before and after exposure to glutaric acid vapor. A spectrum of glutaric acid is given for comparison.

Figure 13 shows temporal profiles of NO₂ uptake and HONO production on 3 mg of Type B propane soot sample before (Figure 13a) and after being coated with glutaric acid for 30 minutes (Figure 13b) by heating the bottom part of the evacuated container at 85 °C. The NO₂ uptake measurements for this example indicate similar NO₂ uptake

coefficients and an increase in HONO yield with a ratio of 1.55 for the glutaric acid coated sample with respect to fresh soot sample. Table 3 summarizes NO_2 uptake coefficients (γ) and HONO yields for fresh Type B propane and kerosene soot samples and samples coated with glutaric acid. HONO yield increases were reported with ratios of 1.73 to 1.31 for different propane soot masses with an increase average ratio of 1.48 times that of the fresh sample for all analyzed samples. The kinetic measurements showed that the NO_2 uptake coefficient increased with an average ratio of 1.8 times when compared with the fresh sample. The effect that glutaric acid has on propane soot can be explained from the point of view of the proposed mechanism in section 3.2, with respect to the binding location on soot. It is probable that glutaric acid molecules bind preferentially on adsorption sites other than $\{S_1\}$, such as $\{S_2\}$, blocking other disproportionation processes (equations 14 and 15), favoring processes in equation 11 and 12 to take place more efficiently and leading to higher HONO yields. Also, it is possible that the glutaric acid blocks the sites where HONO can be irreversibly adsorbed on fresh soot, allowing for more HONO to be released to the gas-phase and leading to higher observed HONO yields. In contrast, Type B kerosene soot samples coated with glutaric acid shows lower HONO increases with an average ratio of 1.14. It is probable that the organic fraction may effect the binding location for glutaric acid in this type of soot, since in section 3.1 (Figures 3 and 4) we found that kerosene flame soot may contain more condensable matter compared to propane flame soot. As a consequence, the effect in HONO yield was not significant. Pre-heated Type B kerosene soot samples showed higher HONO yields when compared with Type B propane soot samples in

Figure 8. Coating experiments with succinic acid are summarized in Table 4. Coating Type B propane and kerosene soot samples with succinic acid showed an increase in HONO yields by a factor of 2.9 and 1.33, and increased NO_2 coefficient by a factor 2.79 and 1.56 respectively.

A temporal profile of NO_2 uptake and HONO production on 2 mg of Type B kerosene soot sample, fresh and coated with sulfuric acid (H_2SO_4) is shown in Figure 14. For this soot sample HONO yield decreased from 72% for fresh soot to 19% for H_2SO_4 -coated soot. Sulfuric acid coating experiments are summarized in Table 5 for Type B propane and kerosene soot samples. These coating experiments were carried out by exposing the soot sample to H_2SO_4 vapor at 85 °C in vacuum with a small helium flow. The coating of both types of soot with sulfuric acid vapor showed a decrease with an average ratio (coated over fresh) of 0.61 for the HONO yield and 0.77 for NO_2 uptake coefficient. For Type B kerosene soot samples the HONO yield decreased by a factor of 0.28 whereas the NO_2 uptake coefficient remained practically unchanged. Lower uptake coefficients may result from a decreased number of available sites due to H_2SO_4 adsorption, leading to lower HONO yields. These results are consistent with those found by Kleffmann et al.⁴⁴ who have shown that when a commercial carbon sample was coated with H_2SO_4 , the HONO yields decreased to nearly zero and the yield of NO increased. They argue that the observed variation in the HONO and NO yields in the reaction of NO_2 with soot coated with H_2SO_4 was caused by an increasing reactivity of the intermediate HONO on the modified surface leading to the decomposition of HONO to NO. In the present study products other than HONO were not monitored.

Exposing sulfuric acid-coated soot sample to 100% relative humidity (RH) caused HONO yield to decrease to 0% for the 2 mg of Type B kerosene soot (Figure 15a) and NO₂ uptake coefficient remain close to that for fresh soot. The sulfuric acid coating on soot may attract water molecules (i.e., high hygroscopicity) from the surrounding environment through absorption, which lead to better sulfuric acid coverage (re-distribution) on the sample soot surface. Therefore, no HONO formation was observed. However, pre-heating the same coated soot sample up to 200 °C restored the HONO production on soot with a HONO yield of 21% and the uptake coefficient did not change. Zhang et. al.⁵⁵ and Pagels et. al.⁵⁶ have shown that soot particles exposed to sulfuric acid vapor followed by heating cause changes in their morphology. It is possible that morphology changes in the soot particles forming the film explain why not complete restoration of HONO production in sulfuric acid-coated soot was observed after heating.

Pyrene coating experiments are summarized in Table 6 for Type B propane and kerosene soot samples. These coating experiments were carried out by exposing the soot sample to pyrene vapor at 100 °C in vacuum with a small helium flow. Uptake experiments before and after coating with pyrene showed no significant trend in both types of soot. Pyrene is a polycyclic aromatic hydrocarbon (PAH) consisting of four fused benzene rings, resulting in a flat aromatic system and can also be produced from the incomplete combustion of fossil fuels. Since soot is found to have amorphous graphitic-like structure it was expected that pyrene molecules would be able to readily adsorb on the soot surface and have a large effect in decreasing HONO yield and NO₂ uptake coefficient. Kubicki et al.⁵⁷ in a theoretical study shows that interaction between

PAHs and soot occurs mainly through π - π system van der Waals forces, implicating that larger and more aromatic molecules will have a higher attraction to soot. A possible explanation for not observing a clear trend is the small and variable surface coverage since the vapor pressure of pyrene is very low.

3.4. Possible Atmospheric Implications

In order to analyze the possible impact of the heterogeneous reaction of NO_2 on soot leading to HONO as the major product in a polluted urban environment we carried out a series of long-time NO_2 exposure experiments on Type B propane soot (fresh, pre-heated, and coated with glutaric acid) to calculate what is the total amount of HONO that can potentially be formed per unit surface area of soot (referred also as HONO generation capability of soot). In these experiments the soot sample surface was exposed to NO_2 in one step, by retracting the injector 8 cm in length, nearly one hour with the typical experimental conditions used before: NO_2 concentrations ranging from 5×10^9 to 5×10^{10} molecules cm^{-3} , total 1.5 Torr, and room temperature. Figures 16 and 17a show the flux of HONO molecules as a function of time during an 1 hr exposure of 1.68 mg of Type B propane soot sample to the NO_2 flow, for fresh (Figure 16a), and pre-heated (at 300 °C) soot samples (Figure 16b), and a sample coated with glutaric acid (Figure 17a). After exposure to NO_2 during an hour the soot samples did not deactivate completely and differences in the rate of HONO evolution were observed. The NO_2 reservoir limited the extent of the uptake experiment. However, data points were extrapolated until complete deactivation by fitting the curves with an exponential equation. The instant HONO yield is shown in Figure 17b, displaying that the HONO

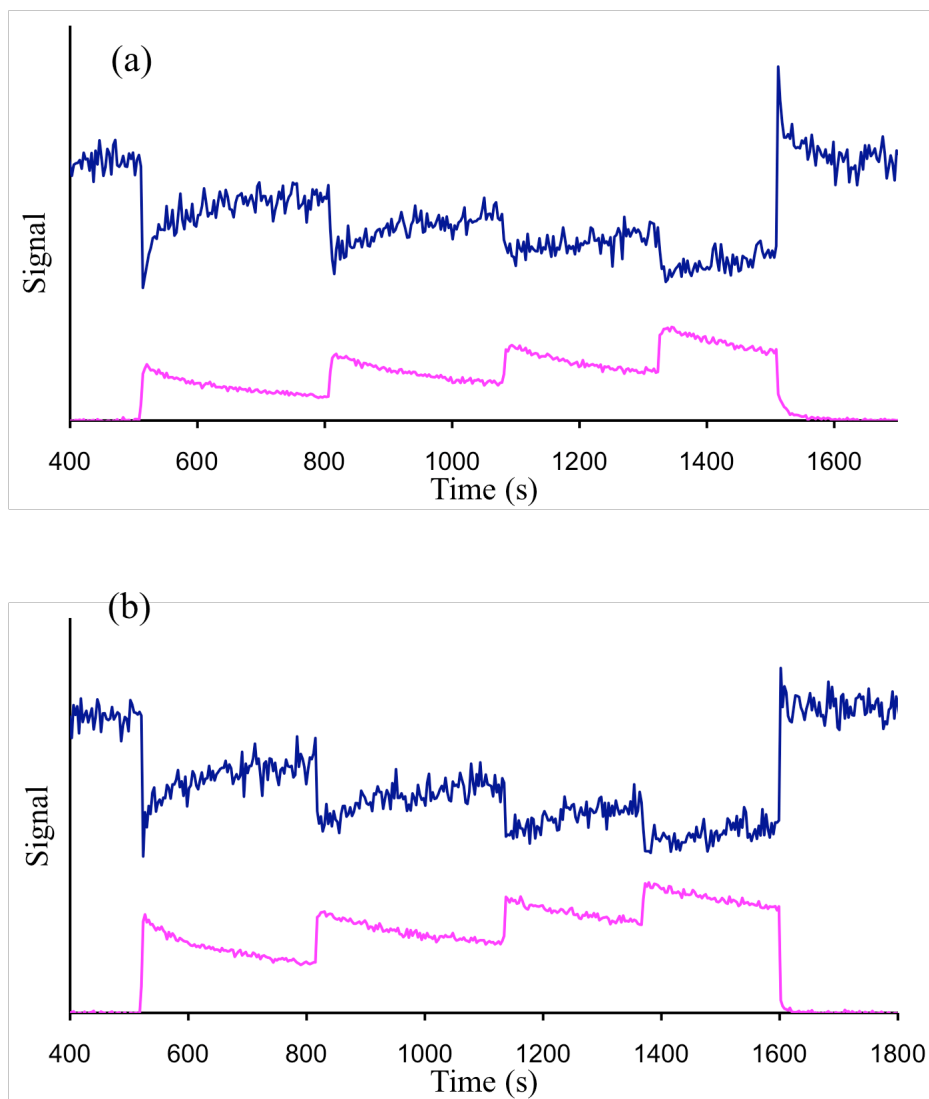


Figure 13. Temporal profile of NO₂ uptake and HONO production on 3 mg of Type B propane soot, fresh (a) and coated with glutaric acid at 85 °C in vacuum for 30 min (b) with stepwise exposure in 2 cm increments up to 8 cm in length. Experimental conditions were $T = 298 \text{ K}$, $P = 1.5 \text{ Torr}$, $U = 134 \text{ cm s}^{-1}$ and $[\text{NO}_2] = 1 \times 10^{10} \text{ molecules cm}^{-3}$. The injector was returned to its original position after $\sim 1550 \text{ s}$ for plot (a) and 1600 s for plot (b). HONO yield increase from 57% for fresh soot to 89% for coated soot.

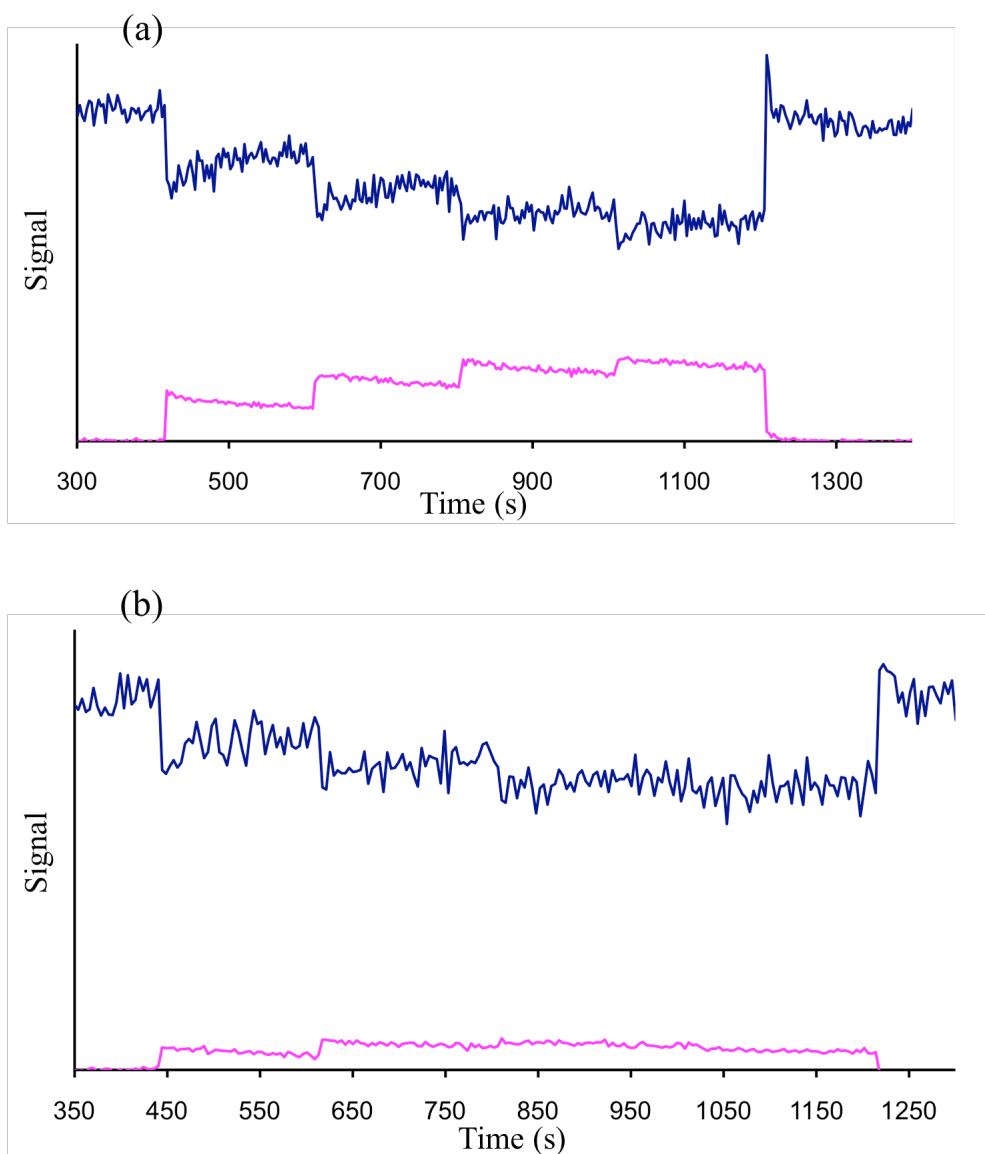


Figure 14. Temporal profile of NO₂ uptake and HONO production on 2 mg of Type B kerosene soot, fresh (a) and coated with sulfuric acid at 85 °C in vacuum for 30 min (b) with stepwise exposure in 2 cm increments up to 8 cm in length. Experimental conditions were $T = 298 \text{ K}$, $P = 1.5 \text{ Torr}$, $U = 134 \text{ cm s}^{-1}$ and $[\text{NO}_2] = 1 \times 10^{10} \text{ molecules cm}^{-3}$. The injector was returned to its original position after $\sim 1250 \text{ s}$ for plot (a), and (b). HONO yield decrease from 72% for fresh soot to 19% for coated soot.

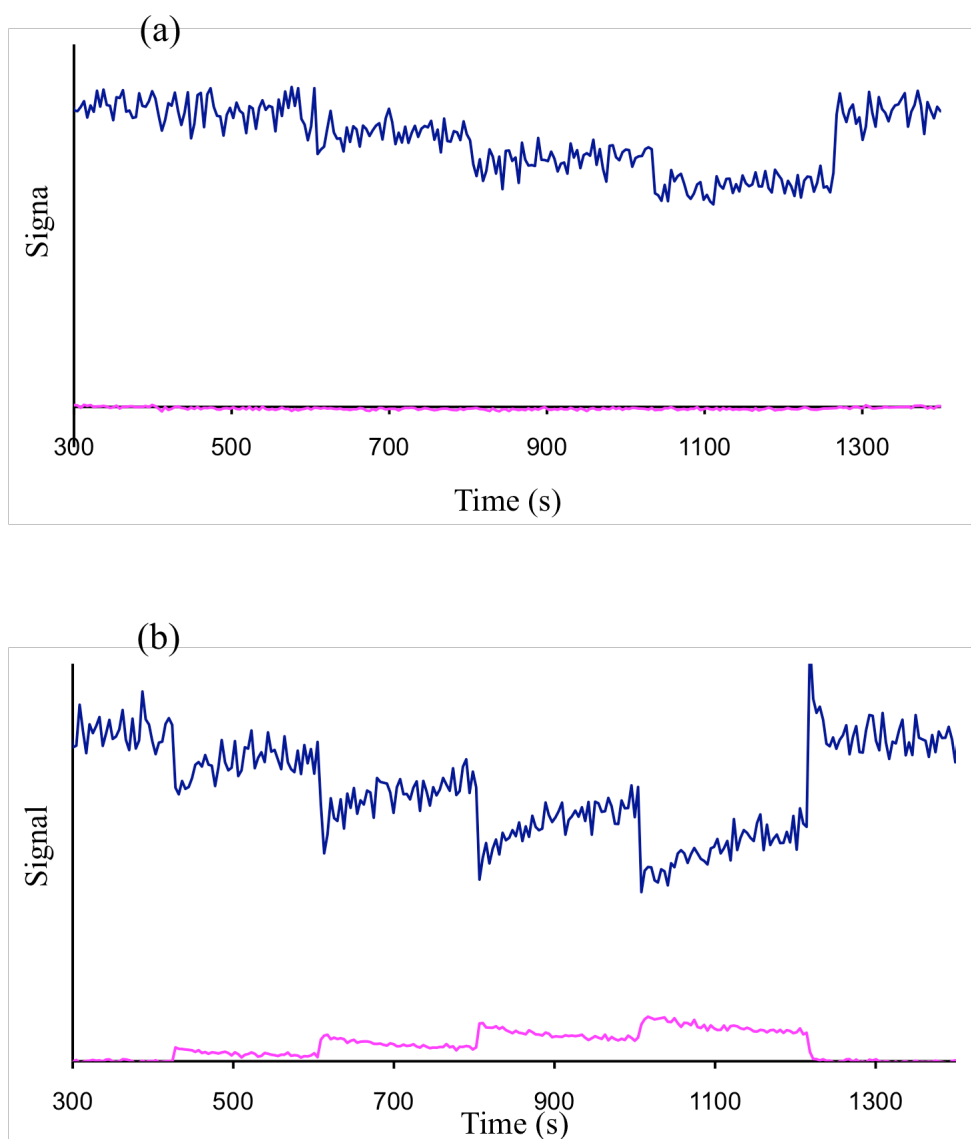


Figure 15. Temporal profile of NO_2 uptake and HONO production on 2 mg of Type B kerosene soot, sulfuric acid-coated soot exposed to 100% RH (a) and pre-heated (b) with stepwise exposure in 2 cm increments up to 8 cm in length. Experimental conditions were $T = 298 \text{ K}$, $P = 1.5 \text{ Torr}$, $U = 134 \text{ cm s}^{-1}$ and $[\text{NO}_2] = 1 \times 10^{10} \text{ molecules cm}^{-3}$. The injector was returned to its original position after $\sim 1250 \text{ s}$ for plot (a), and (b). Heating restored HONO yield on sulfuric acid-coated soot exposed to 100% RH from 0% to 21%.

yield remained constant through the reaction time. By dividing the area under the curve (Figures 16 and 17a) by the BET-surface area of soot the HONO generation capability were calculated. The results obtained are 1×10^{12} molecules cm^{-2} for fresh soot, 8×10^{12} molecules cm^{-2} for pre-heated soot, and 1×10^{13} molecules cm^{-2} for soot coated with glutaric acid. The value reported in this study for fresh soot is much smaller than the values reported in the literature by Aubin and Abbatt (8.2×10^{13} molecules cm^{-2} on n-hexane, benzene and decane soot)⁴³, Kleffmann et al. (8×10^{13} molecules cm^{-2} on lamp black)⁴⁵, and Lelievre et al. (3.1×10^{13} to 4.8×10^{13} molecules cm^{-2} on n-hexane and toluene soot)⁵². A possible explanation for such large difference is the wide variety of different types of soot analyzed, since it have been shown that different types of soot have different physical and chemical properties (surface functional groups) that play an important role in the soot reactivity toward NO_2 . However, using the geometric surface area of soot sample the HONO generation capability increases by two orders of magnitude. The results obtained are 7×10^{13} molecules cm^{-2} for fresh soot, 5×10^{14} molecules cm^{-2} for pre-heated soot, and 1×10^{15} molecules cm^{-2} for glutaric acid-coated soot.

The pre-heated soot sample shows an enhancement in the HONO generation capability of soot by a factor of 6.6 with respect to the fresh soot sample and the glutaric acid coated soot sample shows a larger enhancement of 7.9. An increase in the surface area of soot by heating or coating does not explain such enhancements in the HONO generation capability by itself, which indicate that in effect soot “aging” with glutaric acid and succinic acid could be changing the reaction pathways for HONO formation on

soot. In addition, the instant HONO yield remained constant during the complete reaction time for fresh, pre-heated, and glutaric acid-coated soot samples. With the HONO generation capability of soot and the average BET-specific surface area of Type B propane soot [Levitt et al., 2007] an estimate of how much HONO would be formed under upper limit conditions was carried out. Large soot loading of $20 \mu\text{g m}^{-3}$ with no NO_2 concentration limitation in a polluted urban environment was considered, not taking kinetic issues into consideration. Under these conditions the results are 3×10^7 molecules cm^{-3} for fresh soot, 2×10^8 molecules cm^{-3} for pre-heated soot, and 3×10^8 molecules cm^{-3} for glutaric acid-coated soot, which represent less than 0.1 ppbv of HONO that could be formed. Since these results do not take into consideration kinetic issues that might slow down the rate of HONO formation of soot over several days (deactivation of soot with time), these results represent an upper limit to the amount of HONO that can be produced and therefore do not explain by itself the observed accumulation of HONO during night in polluted urban environments considering soot internal surface area (BET-surface area). However, these results strongly depend on the specific surface area of soot and therefore it is important to further investigate to accurately determine the soot surface area for different types of soot and the possible effect of soot “aging” on it.

Considering the geometric surface area of the soot sample the results are 2×10^9 molecules cm^{-3} for fresh soot, 1×10^{10} molecules cm^{-3} for pre-heated soot, and 3×10^{10} for glutaric acid-coated soot, which represent concentration of HONO in the range of 0.1 to 1.2 ppbv. Therefore, using the geometric surface area of the soot sample (i.e. not considering soot porosity) the heterogeneous reaction of NO_2 on soot producing HONO

as the main product explain the HONO concentration measured during night in polluted environment up to 1.2 ppbv.

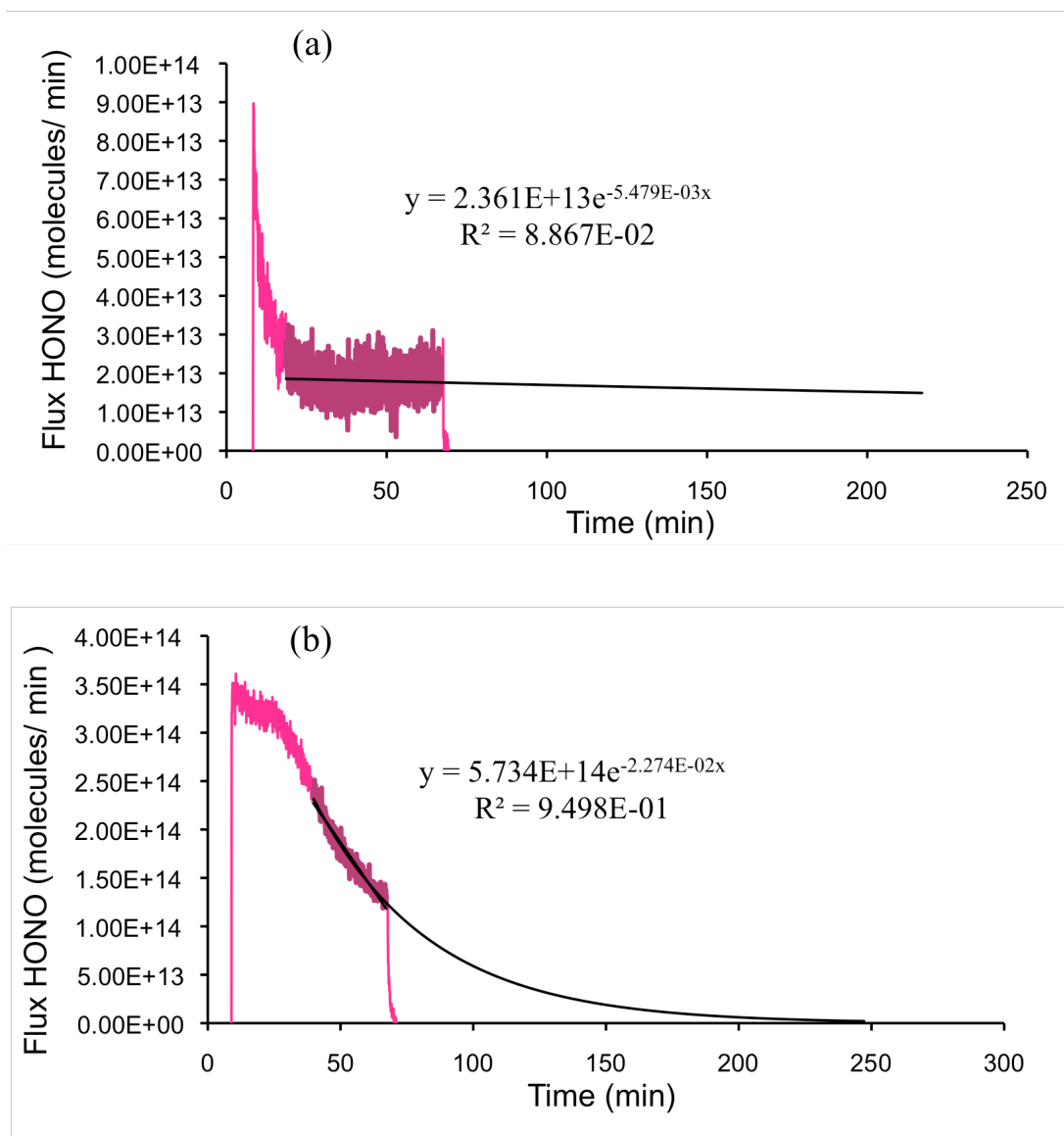


Figure 16. Flux of HONO molecules as a function of time during ~1 hr exposure of 1.68 mg of Type B propane soot to the NO_2 flow, for a fresh (a) and pre-heated soot (b) with initial exposure of 8 cm in length. Experimental conditions were $T = 298 \text{ K}$, $P = 1.5 \text{ Torr}$, $U = 134 \text{ cm s}^{-1}$ and $[\text{NO}_2] = 1 \times 10^{10} \text{ molecules cm}^{-3}$. The injector was returned to its original position after 60 min.

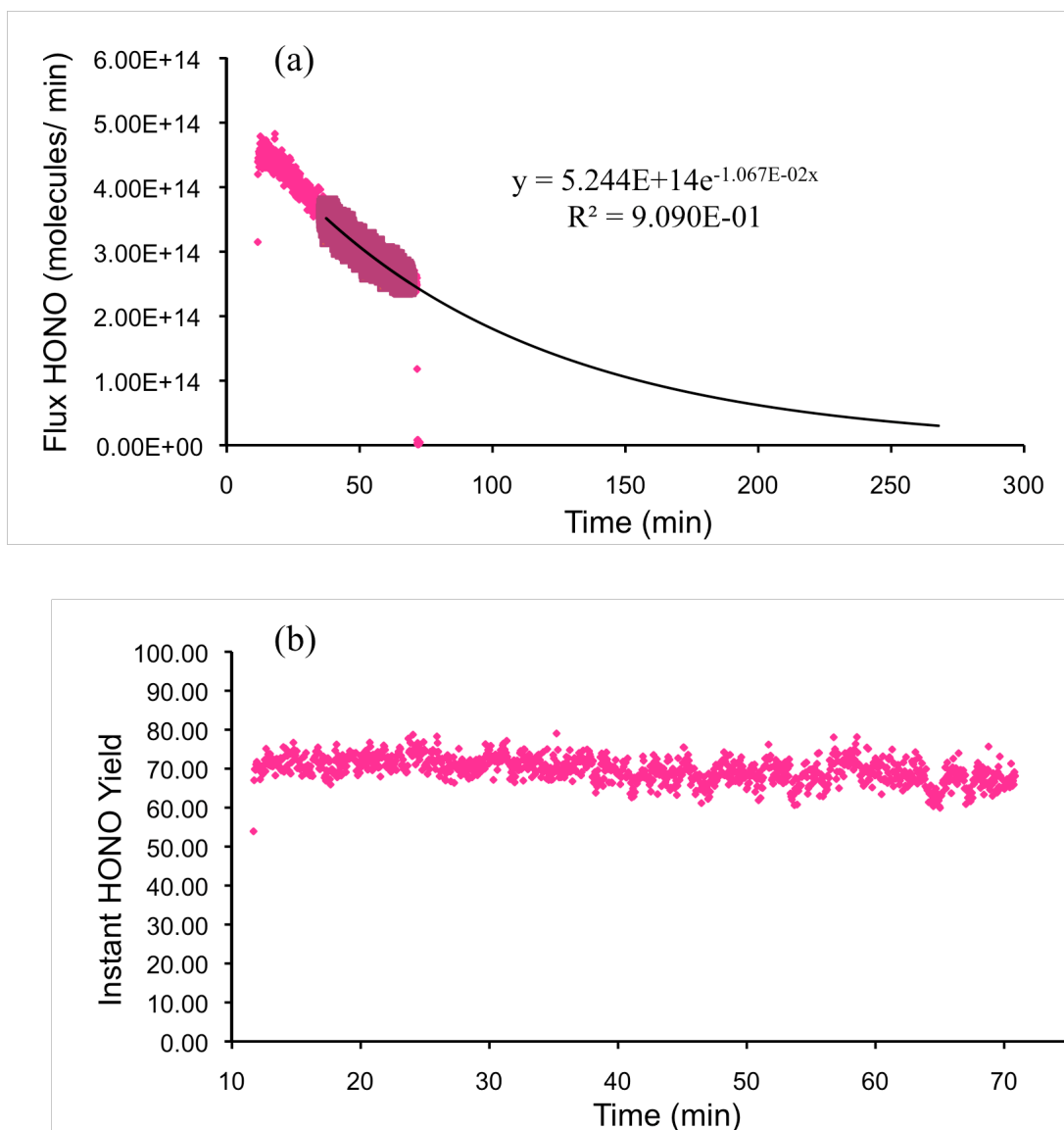


Figure 17. Flux of HONO molecules as a function of time during ~1 hr exposure of 2.88 mg of glutaric acid coated-Type B propane soot to the NO_2 flow (a), and instant HONO yield as a function of time (b) with initial exposure of 8 cm in length. Experimental conditions were $T = 298 \text{ K}$, $P = 1.5 \text{ Torr}$, $U = 134 \text{ cm s}^{-1}$ and $[\text{NO}_2] = 1 \times 10^{10} \text{ molecules cm}^{-3}$. The injector was returned to its original position after 70 min.

Table 3. NO₂ Uptakes Coefficients (γ) and HONO Yields for Fresh Soot and Coated with Glutaric Acid

Type B Propane Soot						
Soot Mass (mg)	γ Fresh	γ Coated	γ Ratio	Yield Fresh	Yield Coated	Yield Ratio
3	2.41E-05	2.29E-05	-0.95 ^a	0.57	0.89	+1.55
4	1.97E-05	6.28E-05	+3.20 ^b	0.49	0.85	+1.73
4	1.93E-05	4.50E-05	+2.33	0.69	1.02	+1.47
9	2.72E-05	3.92E-05	+1.44	0.64	0.85	+1.34
9	3.70E-05	3.94E-05	+1.06	0.76	0.99	+1.31
Average			1.80 ± 0.95 ^c			1.48 ± 0.17

Type B Kerosene Soot						
Soot Mass (mg)	γ Fresh	γ Coated	γ Ratio	Yield Fresh	Yield Coated	Yield Ratio
6	2.01E-05	3.90E-05	+1.94	0.75	0.86	+1.16
4	1.99E-05	2.02E-05	+1.02	0.52	0.59	+1.13
Average			1.48 ± 0.65			1.14 ± 0.02

^a – represent a decrease^b + represent an increase^c Error corresponds to standard deviation (σ)**Table 4.** NO₂ Uptakes and HONO Yields for Fresh Soot and Coated with Succinic Acid

Type B Propane Soot						
Soot Mass (mg)	γ Fresh	γ Coated	γ Ratio	Yield Fresh Soot	Yield Coated	Yield Ratio
9	7.62E-06	2.31E-05	+3.04	0.20	0.52	+2.54
10	8.04E-06	1.01E-05	+1.25	0.29	0.34	+1.17
11	1.49E-06	6.08E-06	+4.08	0.08	0.42	+4.99
Average			2.79 ± 1.43			2.90 ± 1.94

Type B Kerosene Soot						
Soot Mass (mg)	γ Fresh	γ Coated	γ Ratio	Yield Fresh Soot	Yield Coated	Yield Ratio
3	1.07E-05	2.18E-05	+2.05	0.41	0.60	+1.45
10	1.05E-05	1.13E-05	+1.07	0.51	0.62	+1.20
Average			1.56 ± 0.69			1.33 ± 0.17

Table 5. NO₂ Uptakes and HONO Yields for Fresh Soot and Coated with H₂SO₄

Type B Propane Soot						
Soot Mass (mg)	γ Fresh	γ Coated	γ Ratio	Yield Fresh Soot	Yield Coated	Yield Ratio
3	1.29E-05	1.73E-05	+1.34	0.54	0.17	-0.32
3	2.97E-05	1.79E-05	-0.60	0.92	0.71	-0.78
4	1.91E-05	9.81E-06	-0.51	0.70	0.51	-0.74
8	1.46E-05	1.46E-05	1.00	0.57	0.25	-0.45
10	2.25E-05	9.13E-06	-0.41	0.76	0.59	-0.78
Average			0.77 ± 0.39			0.61 ± 0.21

Type B Kerosene Soot						
Soot Mass (mg)	γ Fresh	γ Coated	γ Ratio	Yield Fresh Soot	Yield Coated	Yield Ratio
2	3.36E-05	2.61E-05	-0.78	0.72	0.19	-0.27
8	2.72E-05	2.34E-05	-0.86	0.76	0.13	-0.17
8	6.93E-06	1.14E-05	+1.65	0.34	0.14	-0.41
Average			1.09 ± 0.48			0.28 ± 0.12

Table 6. NO₂ Uptakes and HONO Yields for Fresh Soot and Coated with Pyrene

Type B Propane Soot						
Soot Mass (mg)	γ Fresh	γ Coated	γ Ratio	Yield Fresh Soot	Yield Coated	Yield Ratio
9	1.50E-05	1.49E-05	0.99	0.36	0.41	+1.14
9	1.09E-05	1.59E-05	+1.46	0.36	0.47	+1.31
Average			1.22 ± 0.33			1.22 ± 0.11

Type B Kerosene Soot						
Soot Mass (mg)	γ Fresh	γ Coated	γ Ratio	Yield Fresh Soot	Yield Coated	Yield Ratio
9	2.18E-05	1.44E-05	-0.66	1.00	0.98	-0.95
9	2.59E-05	1.87E-05	-0.72	0.45	0.45	0.99
Average			0.69 ± 0.04			0.97 ± 0.03

4. CONCLUSIONS

In the present work the heterogeneous reaction of NO_2 on different types of soot, leading to HONO formation as the primary product, was studied using a fast-flow reactor couple to CIMS. NO_2 uptake coefficients and HONO yield measurements were performed for propane and kerosene soot samples, both Type A and Type B, as a model of atmospheric soot aerosols. HONO formation correlates to the uptake of NO_2 , indicating that the conversion of NO_2 to HONO on soot surface is a fast reaction. Differences in HONO production were observed for the different types of soot. Type A kerosene fresh soot produced the highest HONO yield, approaching 100% for the samples with small mass. Pre-heating soot sample causes a significant increase in HONO production, independent on the type of fuel or flame regime used during the soot film preparation. HONO yields above 50% were obtained for all pre-heated soot samples and the NO_2 uptake was completely irreversible.

Pre-heating soot samples cause a significant increase in the NO_2 uptake coefficient. The uptake coefficients of NO_2 for the different types of soot varied from 5.6×10^{-6} to 1.6×10^{-4} for fresh soot samples, and from 3.0×10^{-5} to 4.4×10^{-4} for pre-heated soot samples. The observed effect of heating on the reactivity of soot toward NO_2 can be interpreted by the removal of volatile organic fraction from the soot backbone, unblocking surface-active sites, which become accessible for reaction with NO_2 . After heating several soot samples we observed the formation of a thin film of the volatile organic fraction of soot which gradually built-up on the cooler top part of the container.

The uptake coefficients calculated for pre-heated soot samples in this work represent a lower-limit of the actual value due to gas-diffusion limitation.

Yields over 50% discard the surface-catalyzed disproportionation reaction in the presence of adsorbed water as the dominant process for HONO production. However, our results are consistent with an alternative reduction-oxidation mechanism proposed by Ammann et. al.²⁸ and Gerecke et al.²⁸ This heterogeneous reaction mechanism involves a combination of competitive adsorption and reductive centers on soot surface where NO_2 is converted into HONO, and the presence of disproportionation processes on soot where HONO can be decomposed producing other products. In this mechanism soot is considered a reactant rather than a catalyst, since deactivation of soot was observed after exposing the sample for several days in ambient air and no regeneration of soot reactivity was observed after exposing the soot to 100% RH. In the first step-reaction NO_2 is physically adsorbed into an adsorption site (S_1) on the soot surface followed by the second step-reaction where NO_2 reach a reactive site $\{\text{C-H}\}_{\text{red}}$ where it is reduced to HONO by abstraction of a hydrogen atom from the soot surface. Our results showed that the first step-reaction is the rate-limiting step of the NO_2 /soot interaction mechanism for fresh soot samples. However, for pre-heated soot the second step reaction become the rate-limiting step due to an increase in the number of adsorption sites by the removal of the organic fraction from the soot backbone. Therefore the organic fraction condensed on soot backbone play an important role in the HONO formation rate on fresh soot.

Soot-coating, performed to mimic soot “aging” in the atmosphere, affect the reactivity of soot toward NO_2 and HONO formation. Glutaric acid-coated soot increased

both HONO yields with an average ratio of 1.48 times and NO₂ uptake coefficient with an average ratio of 1.8. It is probable that glutaric acid molecules bind preferentially on adsorption sites other than {S₁}, blocking disproportionation processes and favoring the first two step-reactions, leading to higher HONO yields. Similarly, coating Type B propane and kerosene soot samples with succinic acid showed to increase HONO yields by 2.9 and 1.33 respectively.

The coating of both types of soot with sulfuric acid showed a decrease with an average ratio of 0.61 for the HONO yield and 0.77 for NO₂ uptake coefficient. The same trend was observed for Type B kerosene soot samples showing a decrease with an average ratio of 0.28 for the HONO yield. Lower uptake coefficients may result from a decreased number of available sites due to H₂SO₄ adsorption and lower HONO yields may result from the decomposition of HONO on the soot surface. Exposing the H₂SO₄-coated soot sample to 100% RH caused H₂SO₄ to adsorb water molecules and redistribute more uniform through out the soot surface, decreasing the HONO yield near to zero. However, heating the H₂SO₄-coated soot sample partially restore HONO production of soot and no change in the NO₂ uptake coefficient was observed, indicating that morphology changes on soot after coating with H₂SO₄ could be the reason for not complete restoration of the HONO production.

Pre-heated soot and glutaric acid-coated soot increased the amount of HONO that can be formed by unit area of soot by a factor of 6.6 and 7.9 with respect to fresh soot. For a large soot loading of 20 μg m⁻³ and not considering kinetic aspects such as soot deactivation with time in a polluted environment we estimate that HONO concentrations

of 3×10^7 , 2×10^8 , and 3×10^8 molecules cm^{-3} can be produced from fresh, pre-heated, and gutaric acid-coated soot, respectively. These concentrations represent less than 0.1 ppbv of HONO (considering internal surface area of soot) under upper limit conditions and do not explain by itself the HONO concentrations measured during night in polluted urban environments. However, using the geometric surface area of the soot sample explain HONO concentration up to 1.2 ppbv.

In future work it is necessary to investigate whether or not heating or coating of soot samples cause changes in the surface area of soot, since we assumed that the BET-surface area do not change. It is also important to monitor other species that could be formed through different pathways on soot. This could provide more information to improve the mechanism of reaction and understand what is the effect of soot aging in the soot reactivity toward NO_2 and HONO formation. In addition, better control of the combustion condition is required, varying the fuel/oxygen ration in order to associate differences on soot production (surfaces functionalities) with its reactivity toward NO_2 and HONO formation capability.

REFERENCES AND NOTES

- (1) Yu, H.; Kaufman, Y. J.; Chin, M.; Feingold, G.; Remer, L. A.; Anderson, T. L.; Balkanski, Y.; Bellouin, N.; Boucher, O.; Christopher, S.; DeCola, P.; Kahn, R.; Koch, D.; Loeb, N.; Reddy, M. S.; Schulz, M.; Takemura, T.; Zhou, M. *Atmos. Chem. Phys.* **2006**, *6*, 613-666.
- (2) Lance, S.; Nenes, A.; Rissman, T. A. *J. Geophys. Res.* **2004**, *109*, D222208, doi: 10.1029/2004JD004596.
- (3) Nienow, A. M.; Roberts, J. T. *Annu. Rev. Phys. Chem.* **2006**, *57*, 105-128.
- (4) Houghton, J. T.; Intergovernmental Panel on Climate Change. Working Group I. In *Climate Change 2001 : The Scientific Basis: Contribution of Working Group I to the Third Assessment Report of the Intergovernmental Panel on Climate Change*; Cambridge University Press: Cambridge, U.K., 2001.
- (5) Zhang, R. Y.; Suh, I.; Zhao, J.; Zhang, D.; Fortner, E. C.; Tie, X. X.; Molina, L. T.; Molina, M. J. *Science* **2004**, *304*, 1487-1490.
- (6) Bond, T. C.; Streets, D. G.; Yarber, K. F.; Nelson, S. M.; Woo, J.; Klimont, Z. *J. Geophys. Res.* **2004**, *109*, D14203, doi:10.1029/2003JD003697.
- (7) Penner, J. E.; Eddleman, H.; Novakov, T. *Atmos. Environ.* **1993**, *27*, 1277-1295.
- (8) Clarke, A. D.; Weiss, R. E.; Charlson, R. J. *J. Sci. Total Environ.* **1984**, *36*, 97-102.
- (9) Andreae, M. O. ; Andreae, T. W.; Fereck, R. J.; Raemdonck, H. *J. Sci. Total Environ.* **1984**, *36*, 73-80.
- (10) Hansen, A. D. A.; Bodhaine, B. A.; Dutton, E. G.; Schnell, R. C. *Geophys. Res. Lett.* **1988**, *15*, 1193.
- (11) Maricq, M. M.; Xu, N. *J. Aerosol Sci.* **2004**, *35*, 1251-1274.
- (12) Kirchner, U.; Vogt, R.; Natzeck, C.; Goschnick, J. *J. Aerosol Sci.* **2003**, *34*, 1323-1346.
- (13) Saathoff, H.; Moehler, O.; Schurath, U.; Kamm, S.; Dippel, B.; Mihelcic, D. *J. Aerosol Sci.* **2003**, *34*, 1277-1296.

- (14) Hopkins, R. J.; Tivanski, A. V.; Marten, B. D.; Gilles, M. K. *J. Aerosol Sci.* **2007**, *38*, 573-591.
- (15) Kirchner, U.; Scheer, V.; Vogt, R. *J. Phys. Chem. A* **2000**, *104*, 8908-8915.
- (16) Lelievre, S.; Bedjanian, Y.; Pouvesle, N.; Delfau, J. L.; Vovelle, C.; Le Brass, G. *Phys. Chem. Chem. Phys.* **2004**, *6*, 1181-1191.
- (17) Saathoff, H.; Naumann, K. H.; Schnaiter, M.; Schock, W.; Mohler, O.; Schurath, U.; Weingartner, E.; Gysel, M.; Baltensperger, U. *J. Aerosol Sci.* **2003**, *34*, 1297-1321.
- (18) Longfellow, C. A.; Ravishankara, A. R.; Hanson, D. R. *J. Geophys. Res.* **2000**, *105*, 24345-24350.
- (19) Choi, W.; Leu, M. T. *J. Phys. Chem. A* **1998**, *102*, 7618-7630.
- (20) Zhang, D.; Zhang, R. Y.; *Environ. Sci. Technol.* **2005**, *39*, 5722-5728.
- (21) Khalizov, A. F.; Xue, H.; Wang, L.; Zheng, J.; Zhang, R. *J. Phys. Chem. A* **2009**, *113*, 1066-1074.
- (22) Khalizov, A. F.; Zhang, R.; Zhang, D.; Xue, H. *J. Geo. Phys. Res.* **2009**, *114*, 1-15.
- (23) Xue, H.; Khalizov, A. F.; Wang, L.; Zheng, J.; Zhang, R. *Environ. Sci. Technol.* **2009**, *43*, 2787-2792.
- (24) Yao, X.; Fang, M.; Chan, C. K. *Atmos. Environ.* **2002**, *36*, 2099-2107.
- (25) Peng, C.; Chan, M. N.; Chan, C. K. *Environ. Sci. Technol.* **2001**, *35*, 4495-4501.
- (26) Lawrence, J.; Koutrakis, P. *J. Geophys. Res.* **1996**, *101*, 9171-9184.
- (27) Ammann, M.; Kalberer, M.; Jost, D.T.; Tobler, L.; Rossler, E.; Piguet D.; Gaggeler, H. M.; Baltensperger, U. *Nature* **1998**, *395*, 157-160.
- (28) Gerecke, A.; Thielmann, A.; Gutzwiller, L.; Rossi, M. *J. Geophys. Res. Letts.* **1998**, *25*, 2453-2456.
- (29) Lary, D. J. *J. Geophys. Res.* **1999**, *104*, 15,929-15,940.

- (30) Lary, D. J.; Lee, A. M.; Toumi, R.; Newchurch, M. J.; Pirre, M.; Renald, J. B. *J. Geophys. Res.* **1997**, *102*, 3671-3682.
- (31) Febo, A.; Perrino, C.; Allegrini, I. *Atmos. Environ.* **1996**, *30*, 3599-3609.
- (32) Appel, B. R.; Winer, A. M.; Tokiwa, Y.; Biermann, H. W. *Atmos. Environ.* **1990**, *24*, 611-616.
- (33) Lammel, G.; Cape, J. N. *Chem. Soc. Rev.* **1996**, *25*, 361-372.
- (34) Lammel, G.; Perner, D. *J. Aerosol Sci.* **1988**, *19*, 1199-1202.
- (35) Harrison, R. M.; Peak, J. D.; Collins, G. M. *J. Geophys. Res.* **1996**, *101*, 14,429-14,439.
- (36) Kirchsteller, T. W.; Harley, R. A. *Environ. Sci. Technol.* **1996**, *30*, 2843-2849.
- (37) Pitts, J. N.; Biermann, A. M.; Winer, E. C.; Tuazon, M. *Atmos. Environ.* **1984**, *18*, 847-854.
- (38) Pagsberg, P.; Bjerbakke, E.; Ratajczak, E.; Sillesen, A. *Chem. Phys. Lett.* **1997**, *272*, 383-390.
- (39) Finlayson-Pitts, B. J.; Wingen, L. M.; Sumner, A. L.; Syomin, D.; Ramazan; K. A. *Phys. Chem. Chem. Phys.* **2003**, *5*, 223-242.
- (40) Sumner, A. L.; Menke, E. J.; Dubowski, Y.; Newberg, J. T.; Penner, R. M.; Hemminger, J. C.; Wingen, L. M.; Brauers, T.; Finlayson-Pitts, B. *J. Phys. Chem. Chem. Phys.* **2004**, *6*, 604-613.
- (41) Longfellow, C. A.; Ravishankara, A. R.; Hanson, D. R. *J. Geophys. Res.* **1999**, *104*, 13,833-13,840.
- (42) Stadler, D.; Rossi, M. *J. Phys. Chem. Chem. Phys.* **2000**, *2*, 5420-5429.
- (43) Aubin D. G.; Abbatt, J. P. D. *J. Phys. Chem. A* **2007**, *111*, 6263-6273.
- (44) Kleffmann, J.; Becker, K. H. ; Lackhoff, M.; Wiesen, P. *Phys. Chem. Chem. Phys.* **1999**, *1*, 5443-5450.
- (45) Kleffmann J.; Wiesen, P. *Atmos. Chem. Phys.* **2005**, *5*, 77-83.
- (46) Aubin, D. G.; Abbatt, J. P. *J. Phys. Chem. A* **2003**, *107*, 11030-11037.

- (47) Huey, L. G. *J. Phys. Chem.* **1995**, *99*, 5001-5008.
- (48) Keyser, L. F.; Moore, S. B.; Leu, M. T. *J. Phys. Chem.* **1991**, *95*, 5496-5502.
- (49) Zhang, R. Y.; Jayne, J. T.; Molina, M. J. *J. Phys. Chem.* **1994**, *98*, 867-874.
- (50) Zhang, R. Y.; Leu, M. T.; Keyser, L. F. *J. Phys Chem.* **1994**, *98*, 13563-13574.
- (51) Brunauer, S.; Emmett, P. H.; Teller, E. *J. Am. Chem. Soc.* **1983**, *60*, 309-319.
- (52) Lelievre, S.; Bedjanian, Y.; Laverdet, G.; Le Brass, G. *J. Phys. Chem. A* **2004**, *108*, 10807-10817.
- (53) Kalberer, M.; Ammann, M.; Arens, F.; Gaggeler, H. W.; Baltensperger, U. *J. Geophys. Res.* **1999**, *104*, 13825-13832.
- (54) Salgado, M. S.; Rossi, M. J. *Int. J. Chem. Kinet.* **2002**, *34*, 620-631.
- (55) Zhang, R.; Khalizov, A. F.; Pagels, J.; Zhang, D.; Xue, H.; McMurry, P. H. *Proc. Natl. Acad. Sci. U.S.A.* **2008**, *105*, 10,291-10,296.
- (56) Pagels, J.; Khalizov, A. F.; McMurry, P. H.; Zhang, R. Y. *Aerosol Sci. Technol.* **2009**, *43*, 629-640.
- (57) Kubicki, J. D. *Environ. Sci. Technol.* **2006**, *40*, 2298-2303.
- (58) Slowik, J. G.; Cross, E. S.; Han, H. J.; Kolucki, J.; Davidovits, P.; Williams, L. R.; Onasch, T. B.; Jayne, J. T.; Kolb, C. E.; Worsnop, D. R. *Aerosol Sci. Technol.* **2007**, *41*, 734-750.
- (59) Levitt, N. P.; Zhang, R. Y.; Xue, H. X.; Chen, J. M. *J. Phys. Chem. A* **2007**, *111*, 4804-4814.

VITA

Name: Miguel Cruz Quiñones

Address: Department of Atmospheric Science, Texas A&M University,
College Station, Texas 77843-3150.

Email Address: miguelcruz.pr@gmail.com

Education: B.S., Chemistry, University of Puerto Rico at Río Piedras, 2006
M.S., Chemistry, Texas A&M University, 2009